Received: 16 September 2020 | Revised: 3 December 2020 | Accepted: 9 December 2020

DOI: 10.1111/efp.12664

ORIGINAL ARTICLE

Forest Pathology WILEY

Transformation of western hemlock (*Tsuga heterophylla*) tree crowns by dwarf mistletoe (*Arceuthobium tsugense*, Viscaceae)

Stephen J. Calkins | **David C. Shaw** | **Yung-Hsiang Lan**

Department of Forest Engineering, Resources, and Management, Oregon State University, Corvallis, OR, USA

Correspondence
Stephen J. Calkins, Oregon State University, 216 Peavy Hall, Corvallis, OR 97331, USA.
Email: calkins.stephen@gmail.com

Funding information
National Science Foundation, Grant/Award Number: DEB-1440409; Oregon State University

Editor: Jarkko Hantula

Abstract

Dwarf mistletoes (*Arceuthobium* species) are arboreal, hemiparasitic plants of conifers that can change the structure and function of the tree crown. Hemlock dwarf mistletoe (*Arceuthobium tsugense* subsp. *tsugense)* principally parasitizes western hemlock (*Tsuga heterophylla*) and effects 10.8% of all western hemlock trees in Oregon, USA. In this study, we climbed 16 western hemlock trees (age 97–321 years, height 33–54.7 m) across a gradient of infection (0%–100% of branches infected) and measured occurrence of all dwarf mistletoe infections, dwarf mistletoe caused deformities, foliage, branch and crown metrics, and sapwood area. We then modelled over 25 different response variables using linear and generalized linear models with three metrics of severity as explanatory variables: total infection incidence, proportion of all live branches infected, and proportion of all live, infected branches with 33 per cent or more foliage distal to infection. A strong effect of dwarf mistletoe intensification was the reduction of branch foliage and an increase in the proportional amount of foliage distal to infections, with severely infected trees having the majority of foliage distal to infections. Increasing severity led to an apparent crown compaction as crown volumes decreased and became increasingly comprised of deformities. Sapwood area was unrelated to infection severity. Branch length and diameters were unrelated to increasing infection severity despite severely infected branches supporting 1–70 infections. The most severely infected tree had 3,615 individual plants in the crown. Our results suggested that shifts in crown structure and branch deformation, foliage amount, and foliage distal to infection, reflected a likely reduction of capacity for tree growth that coincided with a hypothesized increase in resource demand by dwarf mistletoe plants as infection severity intensified.

KEYWORDS

Arceuthobium tsugense, deformation, dwarf mistletoe, parasitic plant, structure, tree crown, Tsuga heterophylla

1 | INTRODUCTION

Dwarf mistletoes (*Arceuthobium* spp., Viscaceae) are native, flowering, hemi-parasitic plants that can severely impact host structure and function (Glatzel & Geils, 2009; Hawksworth & Wiens, 1996). *Arceuthobium tsugense* subsp. *tsugense* (Rosend.) G.N. Jones infects the crowns of its primary host *Tsuga heterophylla* (Raf.) Sarg. causing deformation to woody tissues and reductions to growth, total foliage, photosynthetic capacity and water use efficiency (Hawksworth & Wiens, 1996; Marias et al., 2014; Meinzer et al., 2004). The most severely infected trees often exhibit dead tops, an abundance of dead branches, and branches supporting several deformities and

numerous infections (Muir & Hennon, 2007). The infection intensification process profoundly transforms the structure of the tree crown and forest canopies as plants increase in number and cause deformation.

There is a large volume of literature on *Arceuthobium tsugense*, mostly focused on managing growth impacts or eliminating and limiting spread into uninfected, younger stands (Geils et al., 2002; Muir & Hennon, 2007; Parmeter, 1978). However, trends in the last several decades of forestry and silviculture have shifted to promoting structural complexity, a focus on resilience, and a recognition of large old trees (Fahey et al., 2018; Franklin et al., 2002; Lutz et al., 2018). Study of older, infected *Tsuga heterophylla* uncovered the extent of impacts to growth and structure, and that these increase over time and severity, and increase susceptibility to abiotic stressors (Bell et al., 2020; Marias et al., 2014; Mathiasen et al., 2008; Meinzer et al., 2004). Ecological benefits derived from their unique structures such as increasing biodiversity and providing bird and mammal habitat were recognized (Griebel et al., 2017; Shaw et al., 2004). Infected trees also play a prominent role shaping local fire dynamics (Shaw & Agne, 2017).

Crown mapping has proved insightful for tree species that create the largest individuals and commonly co-occur with *Tsuga heterophylla* such as *Pseudotsuga menziesii* (Mirb.) Franco, *Sequoia sempervirens* (Lamb. Ex D. Don) Endl., and *Picea sitchensis* (Bong.) Carrière (Ishii et al., 2017; Kramer et al., 2018; Sillett et al., 2010; Van Pelt & Sillett, 2008; Pelt et al., 2004). Crown mapping produces a complete description of a tree's crown architecture and provides valuable data for analysis of crown components such as foliage and branch volumes. Previous crown mapping efforts have not targeted *T. heterophylla* infected with *Arceuthobium tsugense* despite its contribution of unique canopy structures and volume across Northwest forests (Shaw et al., 2004; Van Pelt & Nadkarni, 2004). In Oregon it is estimated 10.8% of all *T. heterophylla* are infected with *A. tsugense* and that 7% of those are moderate or severe (Dunham, 2008). Crown architecture and volume impacts have been more easily studied in forests where tree crowns are more visible or accessible such as in *Pinus contorta* Douglas ex Loudon or *P. ponderosa* Douglas ex P. Lawson & C. Lawson (Agne et al., 2014; Godfree, Tinnin, & Forbes, 2002, 2003; Hoffman et al., 2007). However, these trees also lack comprehensive measurements of the crown's architectural transformation from dwarf mistletoe infection.

In this exploratory study we apply an adapted crown mapping process for the first time to 16 *Tsuga heterophylla* crowns, across a gradient of infection severity (i.e. dwarf mistletoe rating) in mature and old-growth forests at the HJ Andrews Experimental Forest. The adaption will incorporate protocols for measuring infection-induced deformities (Pelt et al., 2004). We assess the impacts to branch form and foliage, crown architecture, and sapwood area due to infection through statistical models of crown mapped data and examine the role deformity class plays in the crown's architecture. Canopy mapping allowed us to use three fine-scale metrics of infection severity as explanatory variables: the proportion of all live branches that are infected (branch severity), the proportion of live branches with 33% or more foliage distal to infection (foliage severity), and the total number of individual infections or *Arceuthobium tsugense* plants (incidence). These took the place of the Hawksworth 6-class dwarf mistletoe rating system in our models as infection severity ratings (Hawksworth, 1977). Lastly, we connected our findings to previous work to bridge gaps between the physical alterations to tree form and its physiological and ecosystem function. We expected branches to have reduced foliage cover as a response to reported reductions in overall infected tree water use, as well as smaller lengths and diameters as infection severity increased. We expected to see a compensatory shift in sapwood associated with decreased foliage area and increasing infection severity. We also expected tree crown volumes to shrink as infection severity increased.

2 | MATERIALS AND METHODS

2.1 | Study site

This research was conducted at the HJ Andrews Long-Term Ecological Research (LTER) site and Experimental Forest (HJA), located in the western Cascade Mountains, northeast of the community of Blue River, McKenzie Bridge, Oregon (44.2°N, 122.2°W) and is part of the Willamette National Forest, administrated by the USFS PNW Research station (https://andrewsforest.oregonstate.edu). Topographical features are representative of the western Cascade Range, with steep mountainous terrain, exposed ridges, sheltered valleys, and a high degree of topographic heterogeneity with elevations ranging from 410 to 1,630 m. Topography and soils have been shaped by volcanic, glacial, fluvial, and other geomorphological processes (Zald et al., 2016). Low elevation soils are characterized by volcanic rock composed of mudflows, ash flows, and stream deposits, transitioning to mostly lava flows as elevation increases (Swanson & Jones, 2002).

Climatic conditions are typical of maritime climates: wet, mild winters and dry, cool summers. Mean temperatures range from 1°C in January to 18°C in July, varying with elevation, aspect, and topographical setting. Precipitation falls primarily from November to March, averaging 2,300 mm/year at low elevations to over 3,550 mm/year at higher elevations. In lower elevations, rain mixed with snow is common during winter and snowpack rarely persists. Snow is more common at higher elevations; above 1,000–1,200 m seasonal snowpack develops, about 1 m in depth.

The sampled trees stand in old and mature forests, below 1,000 m in elevation in the Western Hemlock Vegetation Zone described by Franklin and Dyrness (1973) which comprise the forest community surrounding each tree. Large, old *Pseudotsuga menziesii* dominate the overstory but are spread sparsely throughout the forest. *Tsuga heterophylla* co-dominates in the overstory and *Thuja plicata* Donn ex D. Don is present in the overstory on the wetter sites, in valley bottoms and stream-side. Other characteristics of old-growth such as multi-storied canopy structure and an abundance of dead wood are also common (Spies & Franklin, 1991). Understory

tree species included *T. heterophylla*, *Thuja plicata*, and *Taxus brevifolia* Nutt.. Regenerating trees are almost entirely *T. heterophylla* due to the dense canopies. The most common understory species are *Polystichum munitum* (Kaulf.) C. Presl, *Rhododendron macrophyllum* D. Don, *Mahonia aquifolium* (Pursh) Nutt., *Gaultheria shallon* Pursh, *Vaccinium parvifolium* Sm., and *Acer circinatum* Pursh.

Forest establishment is due to a mix of wildfire and logging. High and mixed severity wildfire is the primary disturbance agent at HJA, with the oldest stands (>500 years old) established post high severity fire (Tepley et al., 2013). Non-stand replacing fires are also common resulting in complex forest structure (Tepley et al., 2013). Forest establishment and disturbance processes are typical of west cascades forests in northwestern Oregon (Spies et al., 2018). *Arceuthobium tsugense* abundance and severity varied by stand, but was always present, even nearby our uninfected trees (see below). Fire and forest structure are the most important controls on dwarf mistletoe occurrence at the landscape scale (Shaw & Agne, 2017). *Arceuthobium tsugense* persists in fire refugia, or in areas of low burn severity, and subsequently reinvades post-disturbance likely creating the landscape distribution pattern present at the HJA (Swanson et al., 2006).

2.2 | Tree selection

We combined lidar data and aerial imagery from the HJA (Spies, 2016), to identify stands of mature and old-growth forest, across the HJA, containing *Tsuga heterophylla*, to opportunistically select our trees, using Spies and Franklin (1991) as a guide. We combined canopy closure values and canopy heights derived from the lidar data to find multistoried stands of non-uniform densities with the tallest trees. Dead tops and severely infected *T. heterophylla* crowns were visible in the aerial imagery which led to final stand selections. Because *Arceuthobium tsugense* abundance and severity are difficult to evaluate from remote sensing data, stands were then surveyed for dwarf mistletoe in person. To capture the full range of infection severity, trees were first rated from the ground using the Hawksworth 6-class dwarf mistletoe rating (DMR) system (Hawksworth, 1977). This involves splitting the live tree crown into thirds and assigning a score of 0, 1, or 2 to each third, and then summing these for a severity rating between 0 and 6. A score of 0 means no branches are infected, a 1 means half the branches or less are infected, and a 2 means more than half the branches are infected with dwarf mistletoe. We selected from suitable trees, picking four trees with a DMR of 0, four with DMR 1–2, four with DMR 3–4, and four with DMR 5–6 for a total of 16 trees. Tree selection criteria also included diameter (>50 cm), height (>35 m), and feasibility and safety of climbing. Dominant or codominant canopy position was another criterion used to select trees that are or were at one point highly vigorous. Individuals with live tops and minimal bole damage or decay were prioritized to minimize confounding effects on crown structure and sapwood responses. At each tree, we inventoried a 10 m fixed-radius plot of trees over 15 cm in diameter for estimating stand composition, stem density, and stand basal area surrounding each tree. No alternate hosts for *A. tsugense*, such as *Abies amabilis* Douglas ex J. Forbes, were present in these stands (Hawksworth & Wiens, 1996).

2.3 | Tree crown measurements

Trees were rigged and then climbed using standard rope climbing techniques emphasizing climber safety; trees with root and butt rot or multiple forks were avoided. We used a simplified version of the whole-tree and crown mapping process described in Kramer et al. (2018), Pelt et al. (2004), and Van Pelt and Sillett (2008) and adapted it to incorporate dwarf mistletoe-related measurements. Before climbing, a functional diameter (*f*-diameter) was established to account for irregularities in ground height or stem form such as buttressing. Functional diameters were established and measured just above irregularities in stem form; if none were present, then diameter was measured at 1.37 m above the ground. Once we accessed the tree crown, the tree height was measured by dropping a fibreglass tape to the ground. This tape was affixed to the treetop and to the corresponding *f*-diameter height to provide a height reference for all branches and coring; once established, branches were measured. Branch measurements included diameter, length, slope, an estimate of foliage cover, and whether branches were live or dead (Table 1). Branch foliage cover estimates were used in place of estimates of foliage area or mass that would have required destructive sampling. Branches smaller than 4 cm in diameter were not measured but were counted. Some long-lived trees are capable of reiteration, where crown architectural units are reproduced within the crown from existing structures, such as branches, after damage to maintain crown function (Ishii et al., 2004). A common example is branches producing upright growths to replace a damaged tree leader. This process was not encountered while measuring and is rare in *Tsuga heterophylla* in general, so all branches are assumed typical of the species unless affected by dwarf mistletoe.

Branches that had developed an infection-related deformity were intensively measured to describe transformations to branch form and assess the impact of deformity volume on host function (Table 2). Deformities were defined as irregularities in typical branch structure caused by an infection such as swellings or witches' brooms (Hawksworth & Wiens, 1996). These could be identified by either living or dead aerial shoots or 'basal cups' left behind where aerial shoots had emerged from the branch and subsequently detached. To calculate infection structure (deformity) volume, a length, width, and depth was measured which was then used to model an ellipsoid. These were measured in the same direction with respect to the branch, for all structures (length parallel to the branch, width perpendicular to the branch, depth perpendicular to those). Deformities with length, width, and depth all less than 4 cm in were not measured but counted.

Surveys of other tree species infected with dwarf mistletoes have found consistently replicated, distinct deformations to branch

TABLE 1 Descriptions of measurement and their units taken on each branch

Variable	Units	Description
Branch Diameter	centimetres	Diameter immediately distal to branch collar
Branch Length	metres	Path length of branch from bole face to tip
Slope 1	degrees	Slope of branch immediately distal to branch collar; initial angle
Slope 2	degrees	Slope of branch, from base of branch to tip of branch or centre of foliage mass at tip.
Branch Foliage Cover	per cent	Per cent of branch length with live foliage attached to the branch
Foliage Distal to Infection	per cent	Per cent of live foliage occurring distal to an infection
Number of Live Branches	count	Number of live branches within the tree
Number of Dead Branches	count	Number of dead branches within the tree
Total Number of Branches	count	Total number of branches within the tree
Proportion of Live Branches	proportion of count	Number of live branches divided by the total number of branches within the tree

TABLE 2 Descriptions of measurements and their units taken on each *Arceuthobium tsugense* induced deformity

Variable	Units	Description
Deformity Distance to Bole	metres	Path length along branch, from bole face to the centre of a dwarf mistletoe deformity
Branch Deformity Volume	cubic metres	Volume of a dwarf mistletoe deformity modelled as an ellipsoid
Proportion of Crown in Deformity	proportion	Total volume of deformities in the tree divided by the total volume of the crown
Dwarf Mistletoe Infections	count	Sum of all dwarf mistletoe deformity volumes within the tree

structure thought to be a characteristic of that host-pathosystem (Geils et al., 2002). While classes have been previously described for non-systemic dwarf mistletoes, they did not adequately capture the deformations we observed in *Tsuga heterophylla* crowns (Geils et al., 2002; Hawksworth, 1961). Deformities were classified using a system we developed, that represented four distinct classes: 'classic broom', 'platform', 'pendulous', or 'spindle' (Figure 1). The same climber classified deformities in all trees to reduce sampling bias and variation. In some instances, deformities were clustered or otherwise difficult to distinguish as arising from an individual infection, so judgement of the climber was used to delineate structures, and to classify and measure them.

2.4 | Crown volume

We utilized derived crown width measurements from crown mapping to capture stochastic differences in tree crown form by modelling 5-m paraboloid frusta for the length of the live crown. The base of the live crown was defined as the lowest living branch (Shinozaki et al., 1964b). Crown widths were calculated from individual branch slope measurements and then averaged in 5-m intervals. These widths were used to model the parabolic frusta and summed for the whole tree. This frusta-summation method estimated smaller crown volumes than the commonly used parabolic method (Van Pelt & North, 1999) and we assume was better suited to the stochastic crowns. The crown volume metrics measured included minimum branch height, crown depth, crown volume, and sapwood area at DBH and live crown base (Table 3).

2.5 | Core sampling

We collected two tree cores at the *f*-diameter and two cores at the base of the live crown from each tree to examine a mechanism for trees to compensate for infection-induced reductions to whole tree water use by measuring sapwood area (Meinzer et al., 2004). Sapwood area may also reflect other alterations to hydraulic architecture such as reductions in foliage (Shinozaki et al., 1964a). We also measured the 10-year basal area increment (BAI) and calculated the relative basal area increment (RBAI) to examine growth trends related to infection severity. All coring was completed during early September 2019 to minimize variation from different seasonal availability of water and bole growth. Diameter of the bole at the coring location was taken at the narrowest point when branches or stem irregularities were present. The sapwood length was measured in the

FIGURE 1 The four deformity classes found within our *Tsuga heterophylla* infected crowns: platform (a), classic broom (b), pendulous (c), and spindle (d). Note the foliage and branchlets of the classic extend away from the bole leaving one side bare while the pendulous has a skirt of foliage all around it. The classic and spindle are both exhibiting secondary infection

TABLE 3 Descriptions of measurements taken on the tree crown and sapwood

Variable	Units	Description
Minimum Branch Height	metres	Lowest live branch on the tree; base of live crown
Crown Depth	metres	Tree height minus the height of live crown base
Crown Volume	cubic metres	Sum of crown volume frusta, modelled as paraboloids in 5-m segments or as a whole paraboloid
Sapwood Area at *f* DBH	square metres	Sapwood area measured from cores taken at the functional breast height
Relative Sapwood Area at *f* DBH	unitless	Sapwood area divided by the total basal area of the tree stem at the functional breast height
Sapwood Area at Live Crown Base	square metres	Sapwood area measured from cores taken at the base of the live crown
Relative Sapwood Area at Live Crown Base	unitless	Sapwood area divided by the total basal area of the tree stem at the base of the live crown

field to avoid drying-related shrinkage. Sapwood was determined by holding the fresh core up to a light source and examining the core for the sapwood–heartwood boundary. These cores were saved for later BAI measurements and cross-dating to determine ages. Occasionally wetwood was encountered in tree cores. Wetwood is a phenomenon in *Tsuga heterophylla* where sapwood is converted to heartwood and then moisture, phenols, and other compounds concentrate there. This results in an abnormally moist portion of heartwood and is often associated with ring shake and defence against rot-associated fungus (Shaw et al., 1995).

2.6 | Analysis

A series of linear (LM) and generalized linear models (GLM) were fit to estimate mean responses among the 16 *Tsuga heterophylla* where branch severity, foliage severity, or incidence were explanatory variables (Table 4). These three measures reflect the process of infection intensification, where ejected seeds land on branches of the original host and infect new branches or reinfect the source branch, increasing incidence and/or severity within a tree crown (Geils et al., 2002). Branch severity was used to represent a fine-scale version of

TABLE 4 Descriptions of the explanatory variables and their units used in the modelling

Variable	Units	Description
Branch Severity	percentage	Number of live, infected branches divided by number of live branches
Foliage Severity	percentage	Number of all live, infected branches with 33% or more foliage distal to infection, divided by the number of live branches
Incidence	count	Total number of infections on live branches within a tree

the DMR system which is the current standard for measuring infection severity (Hawksworth, 1977). Because foliage distal to infection was reported to have reduced physiological function, foliage severity was used to represent where infection impacts would be most strongly associated (Meinzer et al., 2004). Incidence is another way of measuring the intensification process which we compare to the other two measures of severity.

It was not possible to include all explanatory variables in one model and capture their interactions due to limited sample size and power, so all responses were tested with each measure of severity. The general form of the linear and generalized linear model for estimating effects of infection intensification:

$$Y_i = \beta_1(\text{Branch, Foliage Severity, or Incidence}) + \beta_0$$

Estimated values for the coefficient β_1 are presented in Section 3. We fit a quasibinomial GLM for proportion of live branches as the response with a logit link and fit negative binomial GLMs for the number of live branches, number of dead branches, total number of branches, and median number of infections per branch with a natural logarithm link (Ramsey & Schafer, 2012). Slope estimates from the binomial model with a logit link are estimated odd ratios. Slope estimates from negative binomial models with a natural logarithm link are multiplicative changes in mean response. All other responses were modelled by fitting an LM: average, median, and max branch diameter; average, median, and max branch length; average and median branch slope 1; average and median branch slope 2; average branch foliage; average deformity distance to bole; average branch deformity volume; total deformity volume; minimum branch height; crown depth; total crown volume; proportion of crown volume in deformity; sapwood area at *f*-DBH and live crown base; relative sapwood area at *f*-DBH and live crown base.

We then compared each model's fit using the amount of variation explained by the explanatory variables (R^2). To compare different model types, we used the theoretical R^2 for the negative binomial and quasibinomial GLMs (Nakagawa et al., 2017; Nakagawa & Schielzeth, 2013). To determine if *Arceuthobium tsugense* was exhibiting an influence on a specific response, we used a minimum R^2 of 0.20. Forest development processes often lead to surviving trees with individualistic and irregular tree crowns, of which dwarf mistletoe infection is one process (Michel & Winter, 2009; Van Pelt & Sillett, 2008). Additionally, there were no previous studies to suggest what amount of association should be expected with a continuous measure of severity, so we propose an R^2 of 0.2 is an appropriate starting place.

Residuals for the LMs were examined graphically for assumptions of constant variance and normality. Residual versus deviance residual plots were examined for each GLM and no unusual patterns were observed. Overdispersion was checked for each GLM with a negative binomial and binomial distribution. Only the GLM with counted proportion of live branches as the response variable was found to have a high measure of overdispersion (>5.0) and so a quasibinomial correction was used for final analyses and reporting (Ramsey & Schafer, 2012). All analyses were performed using R version 3.6.3 (R Core Team, 2019). Negative binomial GLMs were fit with the MASS package version 7.3-47 (Venables & Ripley, 2002). Theoretical R^2 was calculated for the negative binomial and quasibinomial GLMs using the MuMIn package (Barton, 2019).

3 | RESULTS

Trees in our data set captured a range of age, height and diameter expected in old and mature forests, and the full range of infection severity (Table 5). No evidence of decay was present in the roots of trees and extensive coring revealed no evidence of decay at the base of the live crown and at the *f*-diameter. Tree 12 exhibited a dead top, a common symptom associated with extensive *A. tsugense* infection (Hawksworth & Wiens, 1996). Frequently, models where branch or foliage severity was explanatory variables produced R^2 values larger than those same models with incidence. However, the likelihood of the number of dead branches, was most strongly associated with incidence.

3.1 | Branch modelling

Changes in mean average branch foliage, followed by branch slopes 1 and 2 were best estimated by dwarf mistletoe branch and foliage severity models (Table 6). The number of live and dead branches reported the next strongest R^2 values, although they were below the 0.2 threshold (Appendix A). The proportion of live branches, total number of branches had weak associations ($R^2 < 0.2$), and branch diameter and length were reported very weak relationships ($R^2 < 0.1$).

TABLE 5 Characteristics of the 16 *Tsuga heterophylla* sample trees arranged by age, with tree height, functional diameter, density of all trees around each sample tree, basal area of the stand surrounding each sample tree, crown volume, branch severity (the proportion of all live branches infected), foliage severity (the proportion of all live branches with 33% or more foliage affected by infection), incidence (total number of individual infections on live branches), and dwarf mistletoe rating (DMR)

Tree	Age	Tree Height m	f-Diameter cm	Density t/ha	Basal area m^2/ha	Crown volume m^3	Branch severity %	Foliage severity %	Incidence	DMR
1	97	48.8	96.0	159	8.70	1,955.0	0	0	0	0
2	116	46.6	76.5	191	9.30	1,658.8	0	0	0	0
3	125	35.5	63.1	223	23.40	1,864.8	0	0	0	0
4	144	43.8	71.8	318	9.20	1,813.0	58	23	427	5
5	145	40.4	58.5	350	34.00	980.7	100	100	875	6
6	160	51.6	85.8	95	4.90	1,551.4	100	100	1,489	6
7	163	42.7	82.2	159	24.50	2,123.2	100	98	3,615	6
8	164	40.5	67.5	350	37.20	1,803.6	89	57	786	6
9	174	38.6	60.5	255	52.50	2,086.7	75	38	764	5
10	176	46.8	83.8	446	36.70	1,923.0	73	58	1,479	5
11	179	44.4	81.2	64	4.50	1,335.2	16	1	23	2
12	207	49.2	96.3	127	12.80	520.7	100	97	813	6
13	221	48.7	82.5	637	103.20	947.2	64	52	662	5
14	222	54.7	104.5	159	80.30	1,651.4	25	0	69	3
15	250	33.0	70.1	255	12.50	698.7	100	100	1,405	6
16	321	52.0	83.1	191	14.90	2,718.7	0	0	0	0

Note: DMR was calculated from crown map data, not ground-based estimates, following methods described in Hawksworth (1977).

TABLE 6 Results from modelling for the set of branch-related response variables

Response	Model Type	Fixed Effect	Coefficient Estimate	Low 95% CI	High 95% CI	*F*	*df*	*p*	R^2
Average Branch Foliage	LM	Foliage Severity	−13.39	−19.27	−7.51	23.82	1, 14	0.000	0.63
Average Slope 1	LM	Branch Severity	7.02	−0.56	14.61	3.95	1, 14	0.067	0.22
Median Slope 1	LM	Branch Severity	7.04	−0.40	14.48	4.11	1, 14	0.062	0.23
Median Slope 2	LM	Foliage Severity	−13.51	−28.81	1.80	3.58	1, 14	0.079	0.20

Note: The fixed effect with the highest degree of evidence (measured by R^2) of the three is listed with the estimated slope, 95% confidence intervals, test statistics and R^2. Coefficient estimates represent a shift in response variables for a change in severity of 0%–100%. Full set of model results in Appendix A.

We estimated a reduction in mean average branch foliage of −13.39 per cent (95% CI −19.27, −7.51) for the foliage severity model as infection severity increased from 0 to 100 per cent ($R^2 = 0.63$, Figure 2).

Results from branch slope modelling showed crown profiles may be compacting, losing typical conical shape as they became more severely infected with *Arceuthobium tsugense*. Branch severity models of mean average and median slope 1 estimated an increase in slope angle of 7.02 (95% CI −0.56, 14.61) and 7.04 (95% CI −0.40, 14.48) as severity increased from 0 to 100 per cent, respectively ($R^2 = 0.22$ and 0.23). Foliage severity similarly estimated an increase but with a weaker relationship. Meanwhile, foliage severity models of median slope 2 estimated a decrease in slope angle of −13.51 (95% CI −28.81, 1.80) as severity increased from 0 to 100 per cent ($R^2 = 0.20$). Branch severity also estimated a decrease, but with a weaker relationship; incidence reported a weak relationship for all three of these estimates.

Results from both our branch and foliage severity models estimated similar changes to the number of live and dead branches (Figure 3, Appendix A). A 0.76-fold (95% CI 0.55, 1.06) reduction in the mean number of live branches was estimated by the branch and foliage severity models, as severity increased from 0 to 100 per cent. Our branch severity model estimated a 1.36-fold (95% CI 0.89, 2.08) increase and our foliage severity model estimated a 1.37-fold (95% CI 0.92, 2.04) increase in the mean number of dead branches, as severity increased from 0 to 100 per cent. However, these estimates showed weak evidence of correlation. R^2 values for the branch severity models were 0.14 for the number of live and 0.11 for the number of dead branches; for the foliage severity models were 0.14

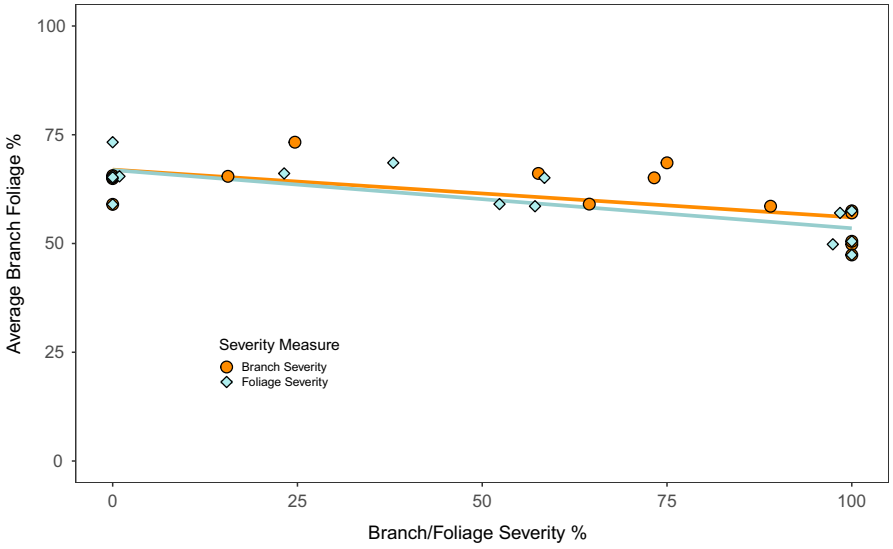

FIGURE 2 Models of mean average branch foliage cover with branch severity (orange lines, % live branches with infection) and foliage severity (blue lines, % live branches with 33% or more foliage affected by infection) as explanatory variables. Raw data are plotted alongside models with branch severity (orange circles) or foliage severity (blue diamonds)

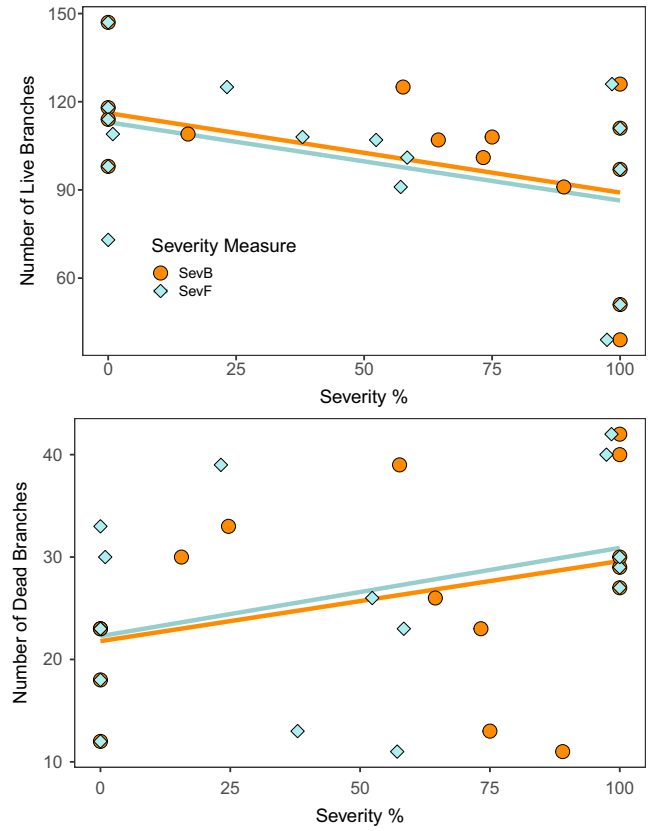

FIGURE 3 Models of mean number of live (top) and dead branches (bottom) with dwarf mistletoe branch severity (orange lines, % live branches with infection) and foliage severity (blue lines, % live branches with 33% or more foliage affected by infection) as explanatory variables. Raw data are plotted alongside models with branch severity (orange circles) or foliage severity (blue diamonds)

for the number of live and 0.13 for the number of dead branches; the incidence model for mean number of live branches did not meet assumptions and an R^2 of 0.14 for number of dead branches was highest among the three explanatory variables. No evidence was found for the estimated decrease in the proportion of live branches ($R^2 \leq 0.01$).

3.2 | Deformity modelling

Deformity-related response variables produced models with our highest degrees of evidence (Table 7, Appendix B). As expected, an increase in branch severity, foliage severity, and incidence was associated with an increase in the median number of dwarf mistletoe infections per branch (Figure 4). The branch severity model estimated branches to experience a 27-fold (95% CI 9.60, 90.06) increase in the median number of infections, as severity increased from 0 to 100 per cent ($R^2 = 0.78$). The model with incidence reported the highest degree of evidence of all incidence models with an R^2 of 0.49.

A small amount of a dwarf mistletoe infected *Tsuga heterophylla* crown volume is comprised of deformities (Figure 5). Total deformity volumes only ranged from 0.56 m^3 to 75.59 m^3 while total crown volumes ranged from 520.70 m^3 to 2,132.20 m^3 in dwarf mistletoe infected trees. We estimated an increase in mean total deformity volume of 55.12 m^3 (95% CI 33.54, 76.70) as foliage severity increased from 0 to 100 per cent ($R^2 = 0.68$). As the total deformity volume in a *T. heterophylla* crown increased, so too did the proportion of the crown comprised of deformities. Foliage severity models estimated an increase of 7 per cent (95% CI 4, 11) in proportion of crown comprised of deformities ($R^2 = 0.57$). However, incidence, branch severity, and foliage severity were estimated to have essentially no effect on the mean average branch deformity volume and exhibited weak evidence for a relationship in those models (Appendix B). Examining the allocation of deformity volume by height showed variation in the location of deformity volume in the crowns of infected trees but appears localized to the mid-crown of the infected trees (Figure 6). The branch severity model estimated an increase in mean average deformity distance to bole of 3.17 m (95% CI 1.62, 4.70), as infection severity increased from 0 to 100 per cent ($R^2 = 0.58$).

3.3 | Deformity class

Deformity class did not exhibit evidence for a relationship to average deformity distance to bole (Table 8). Except for the spindle class,

TABLE 7 Results from modelling for the set of deformity-related response variables

Response	Model Type	Fixed Effect	Coefficient Estimate	Low 95% CI	High 95% CI	*F*	*df*	χ^2	*p*	R^2
Median Dwarf Mistletoe Infection	GLM	Branch Severity	27.20	9.60	90.06	---	1	23.98	0.000	0.78
Total Deformity Volume	LM	Foliage Severity	55.12	33.54	76.70	30.00	1, 14	---	0.000	0.68
Proportion of Crown in Deformity	LM	Foliage Severity	0.07	0.04	0.11	18.85	1, 14	---	0.001	0.57
Average Deformity Distance to Bole	LM	Branch Severity	3.17	1.62	4.70	19.43	1, 14	---	0.001	0.58

Note: The fixed effect with the highest degree of evidence (measured by R^2) of the three is listed with the estimated slope, 95% confidence intervals, test statistics and R^2. Coefficient estimates represent a shift in response variables for a change in severity of 0%–100%. Full set of model results in Appendix B.

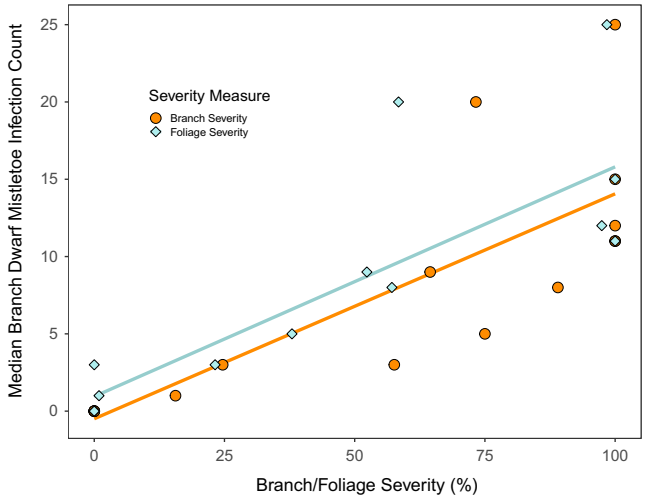

FIGURE 4 Models of median number of dwarf mistletoe infections per branch with dwarf mistletoe branch severity (orange lines, % live branches with infection) and foliage severity (blue lines, % live branches with 33% or more foliage affected by infection) as explanatory variables. Raw data are plotted alongside models with branch severity (orange circles) or foliage severity (blue diamonds)

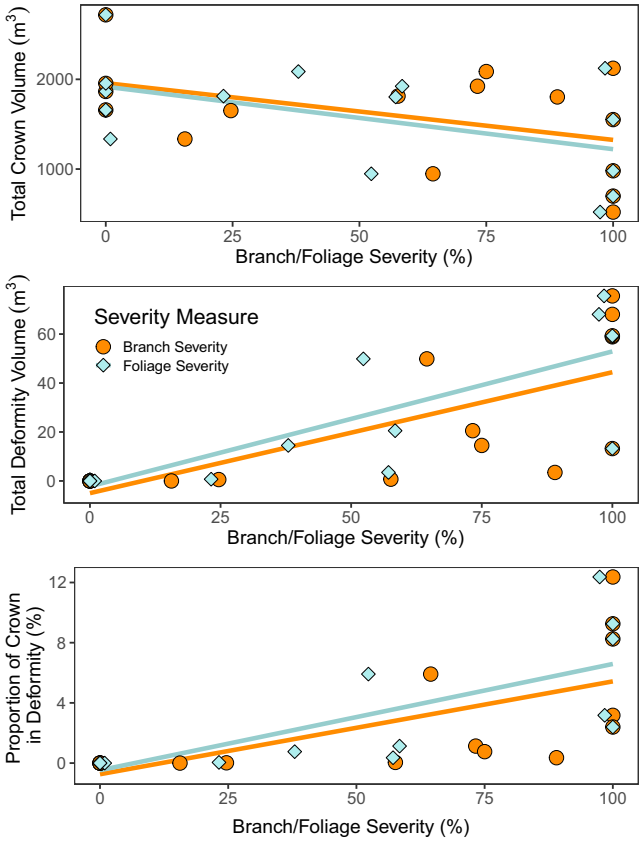

FIGURE 5 Models of mean total crown volume (top), total deformity volume (middle), and proportion of crown composed of deformities (bottom) with branch severity (orange lines, % live branches with infection) and foliage severity (blue lines, % live branches with 33% or more foliage affected by infection) as explanatory variables. Raw data are plotted alongside models with branch severity (orange circles) or foliage severity (blue diamonds). As infection severity increases, volume of the tree's crown decreases and total deformity volume increases resulting in an increased proportion of crown volume filled by deformities

deformity class had negligible effects on mean average deformity volume. Of the deformities large enough to measure volume (≥4 cm in one dimension), we counted 932 classic brooms, 724 platforms, 400 pendulous-shaped, 7 spindle-shaped, and 1 bole infection across all trees. The spindle class represented the smallest amount of total volume of all the classes and were smallest on average, but they were much more abundant than it appears because they were small and we only tallied incidence for small infections. A pendulum infection created the largest max volume of any deformity. The four classes were also found at least 2.51 m from the bole on average.

3.4 | Crown, whole tree, sapwood, and RBAI modelling

Every model with incidence as an explanatory variable showed almost no evidence for a relationship to total crown volume, crown depth, minimum branch height, and relative or absolute sapwood area (Appendix C). Models estimating changes in mean total crown volume with dwarf mistletoe branch and foliage severity as

explanatory variables, exhibited our strongest evidence for a relationship in this set of responses (Table 9, Appendix C). Both estimated similar reductions in mean total crown volume of −632.87 m^3 (95% CI −1330.30, 64.57) for branch severity and −696.34 m^3 (95% CI −1357.10, −35.58) for foliage severity as infection severity increased from 0 to 100 per cent (Figure 5, top). Total crown volume and volume allocation by height showed a wide variation, regardless of dwarf mistletoe infection severity. Like deformity volume, crown volume appeared to be concentrated in the lower and middle thirds of the crown, across the infection severity gradient (Figure 7).

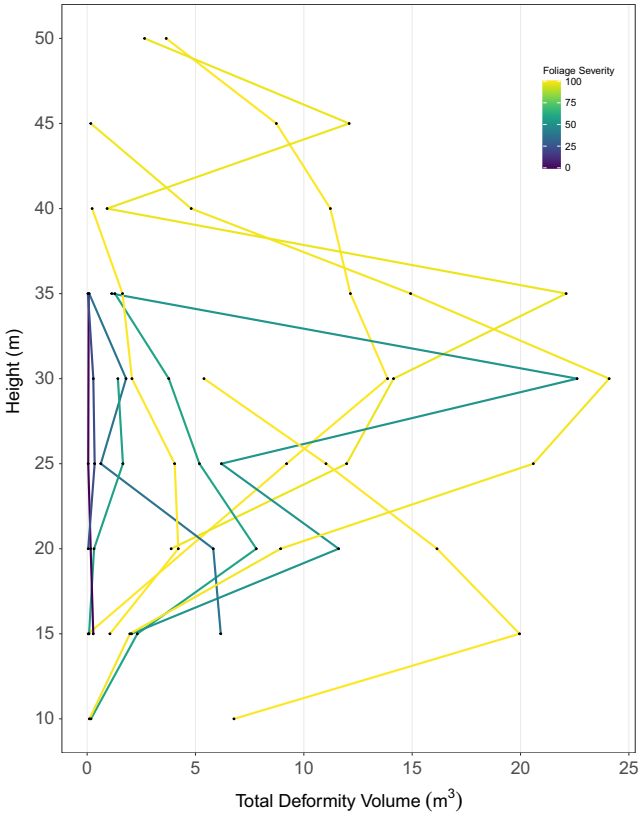

FIGURE 6 Deformity volumes summed at 5-m intervals and plotted against their height. Each 5-m mark on the vertical axis represents the 5 m below it. Each line represents one of the 12 infected trees in this study, coloured by their foliage severity (% live branches with 33% or more foliage affected by infection) where yellow colours are highest severity and blues and purples are lowest severity. Each data point represents a deformity volume summation. Trees varied widely where the deformity volume was located within the crown, but most of the volume was concentrated in the middle third of the crown

In addition to estimated reductions in mean total crown volume, crown depth is also estimated to decrease as dwarf mistletoe branch and foliage severity increases (Table 9). We estimated a reduction in mean crown depth of −6.25 m (95% CI −13.19, 0.70) as infection severity increased from 0 to 100 per cent ($R^2 = 0.21$). Mean minimum branch height was estimated to increase but showed weak evidence for a relationship to infection severity in our models ($R^2 \leq 0.07$). Both results suggested branches may be thinned from below as infection severity increases.

Models of relative sapwood area at *f*-diameter and at live crown base had almost no evidence for a relationship ($R^2 \leq 0.01$) while estimating practically insignificant reductions in area (Appendix C). Models of mean absolute sapwood area produced higher, but still weak degrees of evidence ($R^2 \leq 0.11$). The models of mean absolute sapwood area also estimated a practically insignificant change in area associated with increases in all three explanatory variables. We performed an additional exploratory analysis to examine if the pipe-model theory was evidenced in our sample trees, utilizing the number of live branches as an explanatory variable in place of the area or mass of live foliage. Modelling relative sapwood area at the *f*-diameter and at the base of live crown, with the number of live branches of each tree as the explanatory variable, exhibited stronger evidence for a relationship than branch severity, foliage severity, or incidence (R^2 at *f*-diameter = 0.23, R^2 at base of live crown = 0.33). These models estimated increases in relative sapwood area as the number of live branches increased, without accounting for dwarf mistletoe infection severity or incidence (Figure 8).

Tree RBAI was estimated to decrease with increasing infection severity (Figure 9). Only the model with foliage severity as an explanatory variable met our threshold, with an R^2 of 0.20. This low degree of evidence was likely due to the wide variation in RBAI for uninfected trees, ranging from 0.002 to 0.02, or an exceptionally low to high amount of radial growth. However, all the trees with foliage severity greater than 90% had an RBAI of less than 0.08.

4 | DISCUSSION

From the branch to whole tree level, *Arceuthobium tsugense* exerts a profound influence on *Tsuga heterophylla* trees as infection

Deformity class	*n*	Average volume m^3	Max volume m^3	Average distance to bole m	Average height m
Classic	932	0.19 (±0.28)	2.95	3.49 (±1.56)	26.07 (±9.00)
Platform	724	0.14 (±0.19)	2.83	3.00 (±1.52)	28.39 (±9.28)
Pendulous	400	0.20 (±0.37)	5.74	3.56 (±1.68)	25.93 (±8.29)
Spindle	7	0.003 (±0.001)	0.003	2.51 (±1.54)	17.78 (±5.37)

TABLE 8 Summary table of statistics for each deformity class within infected tree crowns with number observed, average and maximum deformity volume modelled as an ellipsoid, average distance to bole, average height, and their standard deviations listed in parentheses

TABLE 9 Results from modelling for the set of whole tree and sapwood area response variables

Response	Model Type	Fixed Effect	Coefficient Estimate	Low 95% CI	High 95% CI	*F*	*df*	*p*	R^2
Frusta-based Crown Volume	LM	Foliage Severity	−696.34	−1,357.10	−35.58	7.72	1, 14	0.040	0.27
Crown Depth	LM	Branch Severity	−6.25	−13.19	0.70	3.72	1, 14	0.074	0.21
Relative Basal Area Increment	LM	Foliage Severity	−0.01	−0.01	0.00	3.51	1, 14	0.082	0.20

Note: The fixed effect with the highest degree of evidence (measured by R^2) of the three is listed with the estimated slope, 95% confidence intervals, test statistics and R^2. Coefficient estimates represent a shift in response variables for a change in severity of 0%–100%. Full set of model results in Appendix C.

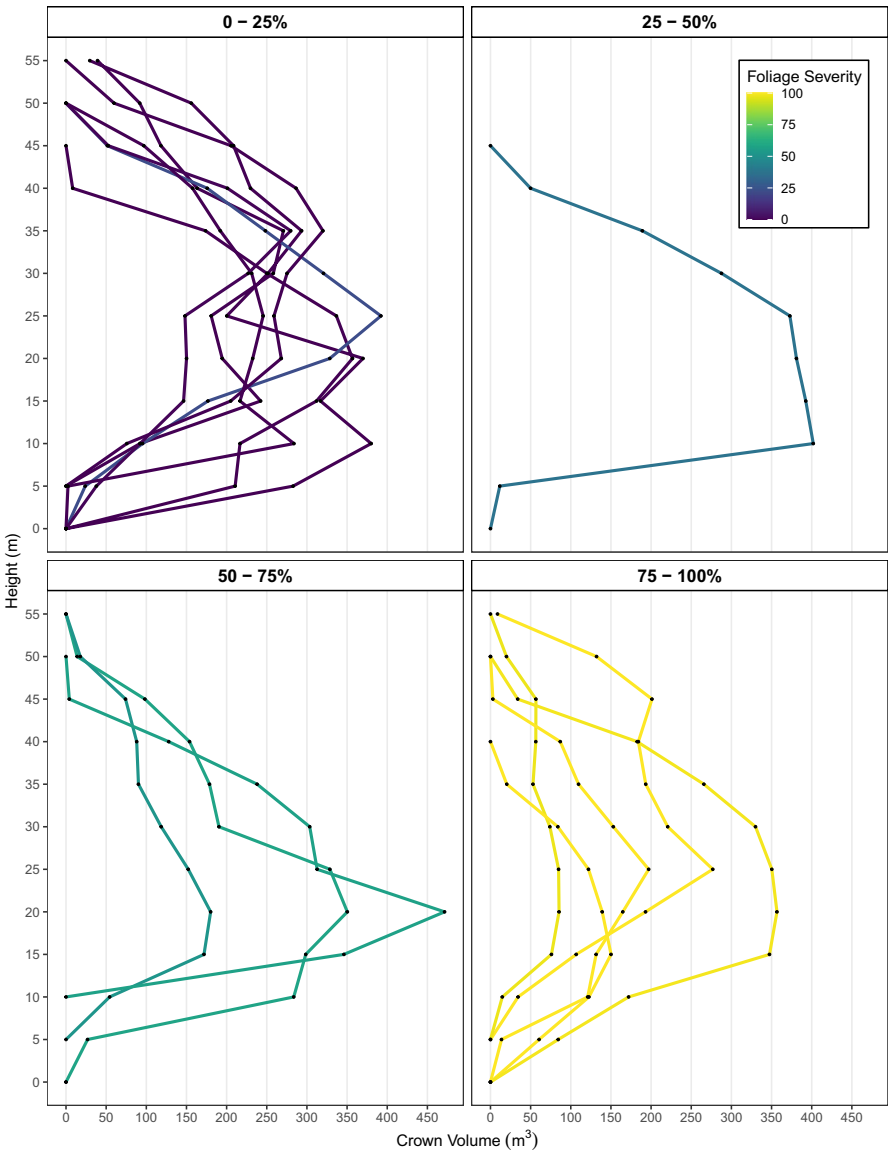

FIGURE 7 Crown volume, modelled as frusta of a paraboloid in 5-m bins, using crown width data, plotted against height of that frusta in the tree. Each 5-m mark on the vertical axis represents the 5 m below it. Each line represents one of the 16 trees in this study and trees have been grouped into 4 groups for ease of viewing, corresponding to their foliage severity (% live branches with 33% or more foliage affected by infection): yellow colours are highest severity, and blues and purples are lowest severity. Each data point represents an individual frustum

intensifies in the tree crown. Infected trees experienced a decrease in average branch foliage cover with increasing infection severity, and in the most severely infected trees, almost all live foliage was located distal to an *A. tsugense* infection. It appeared that altering stem sapwood area was not a compensation mechanism for infected trees to tolerate reduced photosynthetic capacity, as it was unrelated to infection severity. Tree crowns became more compact with increasing infection severity. As infection severity increased we also observed deformation number and total volume increase, while RBAI decreased. Foliage distal to infections have reduced N and photosynthetic capacity (Meinzer et al., 2004) and therefore, as the number of parasitic plants in *T. heterophylla* tree crowns increased,

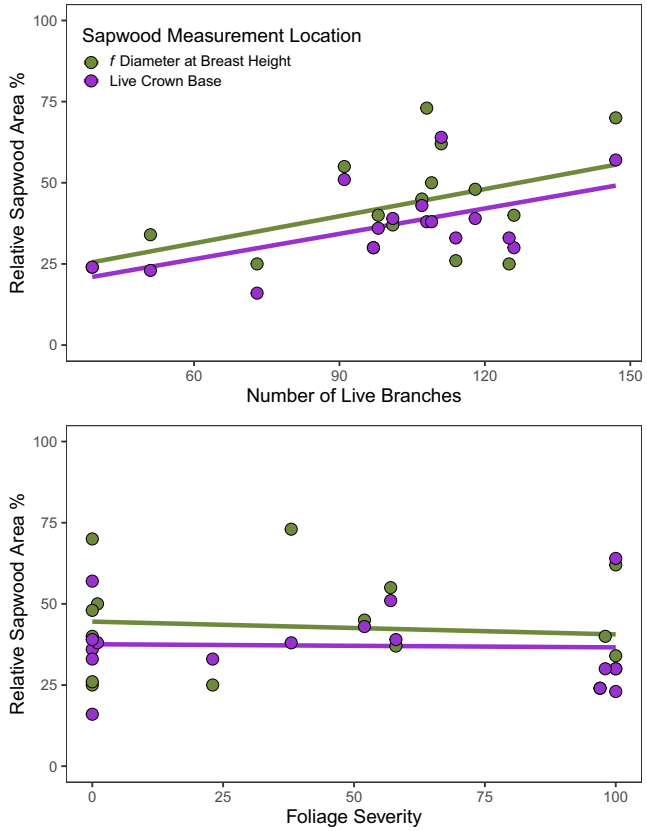

FIGURE 8 Relative sapwood area models with the number of live branches as the explanatory variable (top) and foliage severity (% live branches with 33% or more foliage affected by infection, bottom). Models for the relative sapwood at the functional diameter (green lines and circles) and live crown base (purple lines and circles) are displayed with the raw data

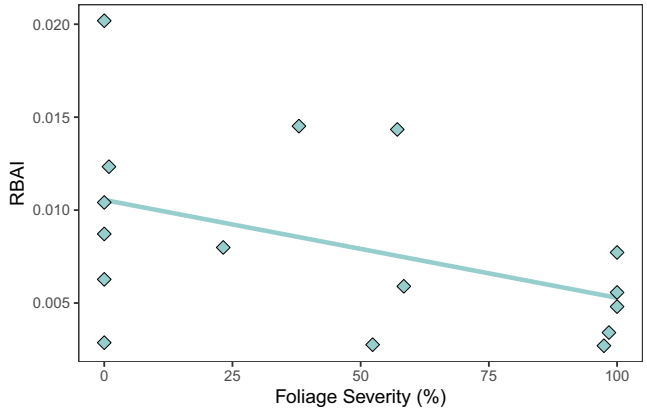

FIGURE 9 Models of relative basal area increment of each tree with dwarf mistletoe foliage severity as the explanatory variable. Raw data are plotted alongside the model with foliage severity (blue diamonds)

the trees likely experienced a reduction in capacity for growth that coincided with an overall reduction in foliage amount and function, and an increased resource demand by *A. tsugense* plants.

This study was exploratory in nature and was the first to apply the canopy mapping process to examine the transformation of mature and old growth *Tsuga heterophylla* crown architecture through a fine-scale gradient of infection severity by *Arceuthobium tsugense*. As such, there was a lack of comparable literature for this present study although *A. tsugense* is well studied (Muir & Hennon, 2007).

4.1 | Foliage impacts

Dwarf mistletoe infections continually influence water and nutrient dynamics in their host, resulting in shifts of hydraulic architecture that allow the tree to maintain some form of water homeostasis (Hawksworth & Wiens, 1996; Meinzer et al., 2004; Sala et al., 2001). Meinzer et al. (2004) observed that old *Tsuga heterophylla* infected by *Arceuthobium tsugense* experienced reductions in branch foliage that preserved leaf-specific conductivity in infected branches and whole tree foliage, likely due to a loss of live branches in infected trees. The remaining branch foliage distal to infection was found to contain almost half the nitrogen, likely influenced by the mistletoe. This decrease in foliage and photosynthetic capacity is thought to render infected trees unable to meet the respiratory demands of live branches and support *A. tsugense* infections during stress events, resulting in branch dieback and reductions in tree growth (Bell et al., 2020; Marias et al., 2014; Meinzer et al., 2004). Our results show compelling evidence that *T. heterophylla* experience reductions in branch foliage cover due to of infection intensification, although the average reduction was only ~13% (Figure 2). Additionally, almost all remaining foliage in 100% branch severity trees was found distal to infections (Figure 10), suggesting these trees are experiencing severely reduced photosynthetic capacity.

While our models also estimated a decrease in live branches and an increase in dead branches, likely resulting in reduced whole tree foliage, we found weak evidence of correlation with infection severity and estimated a wide range of plausible values for the slopes of both models (Figure 3). This suggested, despite the average reduction in branch foliage cover and reduced photosynthetic capacity of remaining needles, infected trees in this study are still capable of meeting the respiratory demands of all branches and that branch mortality may not be a direct result of infection intensification. Maintaining infected branches with ~13% less foliage and significantly reduced photosynthetic capacity, would mean carbon accumulation would be severely limited, resulting in adjustments to allocation. Logan et al. (2013) suggested *Arceuthobium pusillum* Peck infected *Picea glauca* (Moench) Voss dedicate a disproportionate amount of photoassimilate to branches with low water use efficiency, reflected in severely decreased bole diameter growth while significant reductions to bole diameter growth have been demonstrated in infected *Tsuga heterophylla* (Bell et al., 2020; Marias et al., 2014; Shaw et al., 2008) and observed in this study (Figure 9).

Branches of *Tsuga heterophylla* have been reported to be kept alive and foliated, below zones of prohibitively low light where other uninfected branches would have been shaded out (Muir & Hennon, 2007). Further, reductions to whole tree foliage may

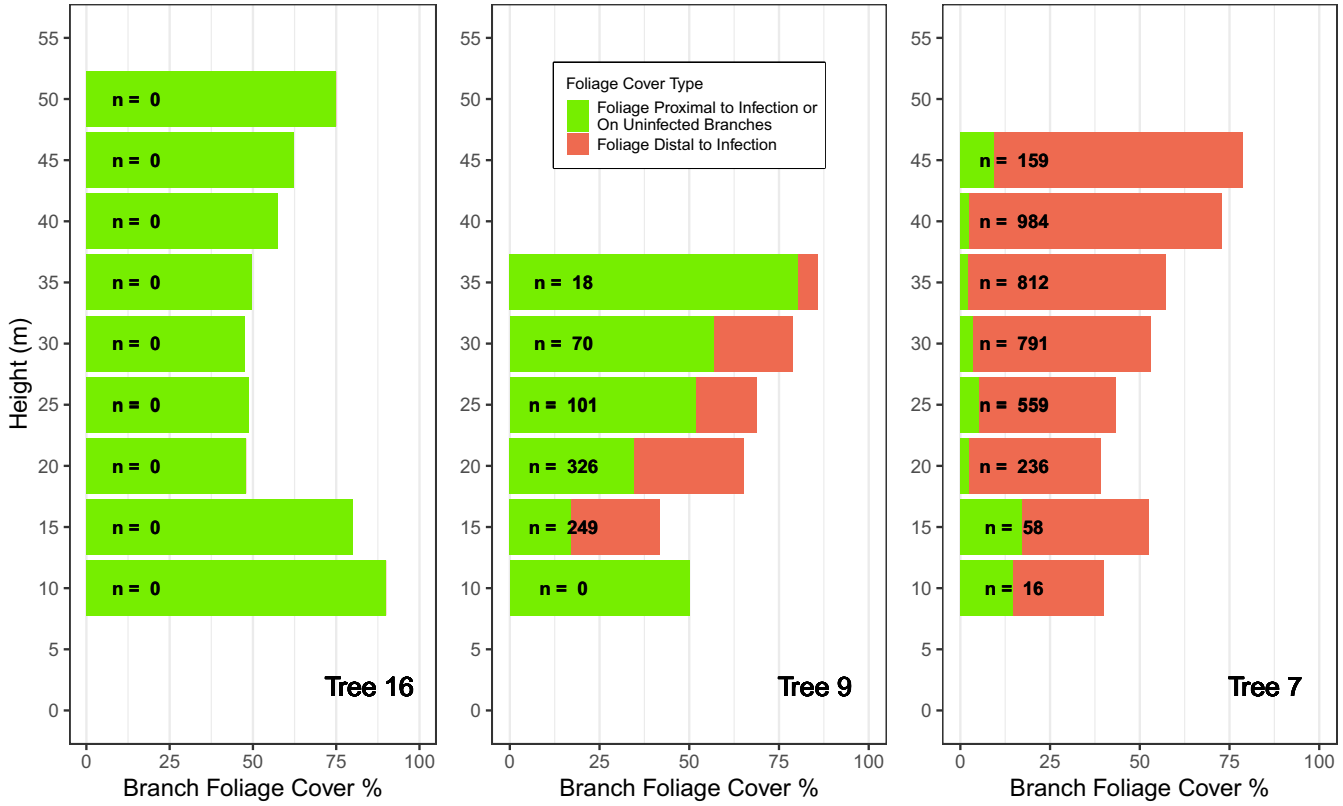

FIGURE 10 Branch foliage cover proximal and distal to infection, or on uninfected branches, stacked, with both summing to total branch foliage cover, averaged in 5-m intervals for the three trees with the largest crown volumes. The *n* represents the number of live infections in that 5-m interval. Trees increase in infection severity from left to right. Trees are labelled with their corresponding tree number and their foliage severity from Table 5

manifest from reductions in individual branch foliage cover across the whole tree. Tree selection bias likely limits the scope of this finding though, as safer trees to climb usually have fewer dead branches and may be more vigorous. Studies, such as Meinzer et al. (2004), that can access severely infected trees without this bias and without felling, may have a more accurate representation of branch mortality.

Foliage impacts are not consistent throughout the other dwarf mistletoe–host pathosystems, though available literature on foliage impacts is limited. Sala et al. (2001) found the opposite effect of our results on foliage when measuring changes to the leaf area: sapwood area ratio of *Pseudotsuga menziesii* infected with *Arceuthobium douglasii* Engelm. which creates a systemic infection, and *Larix occidentalis* Nutt. infected with *A. laricis* (Piper), which creates non-systemic infections, in mixed conifer forests. In both tree species, high infection severity was associated with increases in the leaf area: sapwood area ratio due to increases in leaf area. Godfree et al. (2003), examined how the abundance of *A. americanum* Nutt. Ex Engelm. affected the canopy structure of an old growth *Pinus contorta* var. *murrayana* (Balf.) Engelm. forest in central Oregon. They found severe infections were associated with a stand-wide, skew of foliage distribution to lower heights in the canopy but made no determinations about changes in total foliage mass or area. Most recently Hoffman et al. (2007), in a study on *A. vaginatum's* (Willd.) J. Presl influence on fire in *P. ponderosa* forest stands, found canopy foliage mass remained unchanged despite infection severity. This suggested impacts of a dwarf mistletoe on its host may be specific to the host and pathogen.

Research that tracks branch foliage and mortality over time through infection intensification and can link those to physiological impacts, would provide significant clarity to the impact of *Arceuthobium tsugense* on host growth. Our study only captures a point in time; the time of initial infection is unknown, complicating this picture. The epidemiology of dwarf mistletoe involves spread into new hosts and intensification within the existing host (Hawksworth & Wiens, 1996; Shaw & Mathiasen, 2013). Impacts of infections on host trees change through time as tree infection intensifies. During initial stages of infection, there may be increased growth associated with low severity, but at high severity there is typically severely decreased growth (Marias et al., 2014).

The location of initial infection may also alter the impacts. For example, initial infections lower in the tree crown may be outgrown by *Tsuga heterophylla* as height growth of uninfected tops outpaces the rate of upward spread of infection (Muir & Hennon, 2007). Once height growth slows, total infection of the crown is possible (Robinson & Geils, 2006). Meinzer et al. (2004) also suggested transient changes to the leaf area: sapwood area ratio may have produced apparent discrepancies in tree allometric responses to infection which we could not observe without repeated measurements.

4.2 | Crown structure and volume

Counter to expectations, we did not observe evidence for an effect of increasing infection severity on the mean average, max, or median branch diameter or length. The only study that examined *Arceuthobium tsugense's* effects on *Tsuga heterophylla* branches, measured 30 trees averaging 110 years old from dominant and codominant positions and reported increases in branch diameter, immediately distal to the branch collar, as severity increased (Smith, 1969). Estimates of branch slope angle to tip (slope 2) suggested branch tips end up closer to the tree bole and ground due to increasing infection severity than would be expected for the typical branch arrangement in uninfected trees that maximizes light interception (Smith & Brewer, 1994). Some deformities have been observed to weigh up to several hundred kilograms and this additional weight on the tips of branches may result in a branch droop (Muir & Hennon, 2007). The estimated increased initial branch slope angle (slope 1) with increasing infection severity may be a compensating mechanism for the branch to handle the added weight. Wellwood (1956) observed more compression wood within trees' stems, on the side nearest to infected branches, further suggesting decreased slope 2 angles may be a weight-related phenomenon.

Estimates of decreases in crown depth also run counter to previous findings of changes to crown structure. Previous reviews of *Arceuthobium tsugense's* whole tree effects on *Tsuga heterophylla* have described increasing infection severity may lower the base of the live crown due to branches kept alive below the height where uninfected branches would self-thin (Geils et al., 2002; Muir & Hennon, 2007; Shaw & Agne, 2017). Our results suggested the base of the live crown may actually be increasing in height, although estimates for increases in minimum branch height were not well supported. Decreasing crown depth may also shift canopy volume allocation higher in the trees, despite decreasing branch slope 2 angles, but this was not clear from our findings (Figure 7). The lack of compelling evidence for an effect on branch mortality, which would drive shifts in crown depth, suggested differences in crown depth are more likely attributable to environmental factors than infection severity. For example, tree crowns developed in the presence of nearby dominant trees would likely be less full than crowns developed in full sunlight. We could not investigate stand level effects with 16 trees but a larger sample size across a range of old-growth forests could include these effects in models.

Infection severity exhibited a negative influence on crown volume, although, of the completely infected trees (branch severity = 100%), a wide range of total volumes was observed. The smallest crown volume we observed overall was of a completely infected tree at 520.7 m^3. The largest completely infected crown had a volume of 2,123.2 m^3, second largest overall and the same tree with the highest incidence (Table 5). In all our trees, crown volume allocation by height varied across all infection severities reflecting the stochastic nature of crown development processes in mature and old growth forests (Reilly & Spies, 2015), but crown volume appeared to be greatest in the low to mid crown (Figure 7). Clearly environmental factors, tree vigour, and time since infection are exhibiting influences on the crown volume and structure, but we found evidence to support an overall negative effect of dwarf mistletoe on crown volume. Agne et al. (2014) found strong evidence that in stands of *Pinus contorta* subsp. *murrayana* infected with *Arceuthobium americanum*, canopy volume and cohort height decreased as infection severity increased. Godfree et al. (2002), Godfree et al. (2003) found evidence that individual tree crown volume may be reduced by high severity dwarf mistletoe infections, but that total canopy volume remained constant in their stand due to demographic shifts in tree size classes.

Branch slope, crown depth, and crown volume model results, as well as increased difficulty manoeuvring within the severely infected crowns, suggested an overall compaction of *Tsuga heterophylla* crowns due to increasing *Arceuthobium tsugense* infection severity. The compaction of infected *T. heterophylla* crowns could have implications for biota that utilize deformities for habitat or forage (Hawksworth & Wiens, 1996; Muir & Hennon, 2007), for spread and intensification of *A. tsugense* (Parmeter, 1978; Robinson & Geils, 2006), and for fire and fuels in forests (Shaw & Agne, 2017). *Arceuthobium tsugense's* role in development of old growth structure in Pacific Northwest forests has largely been attributed to gap creation caused by host mortality (Mathiasen et al., 2008; Reilly & Spies, 2016), but compacting crowns as infection severity increased, suggested a continuous process of increasing space between tree crowns before mortality occurs. This would allow more light to reach the forest floor in between trees, especially under the canopies of *T. heterophylla* dominated forests where light penetration is low (Reilly & Spies, 2015).

While crowns were decreased in size and spread, total deformity volume was estimated to increase as infection severity increased, resulting in an increased proportion of crown volume taken up by deformities (Figure 5). Increasing infection severity and total deformity volume did not coincide with an increase in average branch deformity volume, suggesting that infection intensification within the tree crown is the main contributor to total deformity volume and not all infections form large deformities. The lack of effect of infection severity on average deformity volume suggested the development of deformities may be driven instead by light, temperature, or productivity of foliage, all factors important for *Arceuthobium tsugense's* development and related to an infection's height within the canopy (Shaw & Weiss, 2000). Trees with the greatest infection severity had a 27-fold increase in the median number of infections per branch when compared to uninfected trees and we expected that increasing infection incidence would result in increasing branch deformity volume (Figure 4). The distribution of deformity volume within *Tsuga heterophylla* crowns varied by height, independent of infection severity but appeared localized to the low to mid crown (Figure 6), which is consistent with previous studies of dwarf mistletoe brooms (Hawksworth & Wiens, 1996).

Concentration of deformities in the low to mid crown can be a common result of intensification processes (Muir & Hennon, 2007;

Robinson & Geils, 2006). Increasing average deformity distance to bole with increasing infection severity suggested deformity volume becomes localized at the edges of the crown. Branch growth appears unimpeded by infection likely driving this increase in average distance to bole as seeds continue to infect the thin barked segments near the tips. Branch maximum length may then indicate a maximum distance to bole and an eventual maximum crown width of severely infected *Tsuga heterophylla*. In severely infected trees, interior crowns may be mostly branch wood and free space, while the outer shell of the crown is comprised of deformities and effected foliage. This increase in deformity distance from bole also has implications because water path length increases and water transport efficiency of infected branches decreases (Marias et al., 2014; Meinzer et al., 2004).

Estimates of crown volume and biomass are often desired for old trees for carbon accounting and growth modelling as carbon allocation shifts once trees reach old growth stages (Ishii et al., 2017; Kramer et al., 2018; Sillett et al., 2010), or for modelling the development of canopies and how this may relate to the spread of dwarf mistletoe (Robinson & Geils, 2006; Swanson et al., 2006; Van Pelt & Nadkarni, 2004). Allometric models have been produced for young *Tsuga heterophylla*, or uninfected trees in mature and old growth forests, however ours were the first attempt to cover a gradient of dwarf mistletoe infection severity. Further research that expands the sample size and integrates destructive sampling, branch age, and time since infection, with ground-based measurements for predictors could produce more precise models forest managers can use to predict future trajectories of *T. heterophylla* forests infected with *Arceuthobium tsugense*.

4.3 | Deformity class

Arceuthobium tsugense caused-deformities in *Tsuga heterophylla* crowns, took the shape of four distinct classes, depending on where infection occurred on the branch (Figure 1, Table 8). Infections occurring on top of a branch resulted in a spray of foliage perpendicular to the tree (platform); those infecting the main stem of a lateral branch formed a classic witches' broom (classic); those that infected branchlets of primary branches, formed pendulum-shaped deformities that caused the branchlets to droop and foliage to spray out, perpendicularly to the branchlet (pendulous); infections occurring in small branchlets created spindle-shaped swellings commonly associated with early stages of infection (spindle). The classic deformity was the most observed class of deformities larger than 4 cm in one dimension and it is likely that pendulous infections transition into classic deformities with age (Table 8). Deformities smaller than 4 cm in one dimension were not classified, but the vast majority resembled a spindle-shaped swelling, as was expected (Muir & Hennon, 2007).

Previous broom classification systems have been devised for other host–dwarf mistletoe pathosystems although neither match deformities observed in this study. Hawksworth (1961) described three broom growth forms typical of nonsystemic dwarf mistletoes, using *Arceuthobium vaginatum* as a model, determined by distance from the bole: typical, volunteer leader, and weeping, with illustrations in Geils et al. (2002). The typical resembles the classic brooms we found in our trees. The volunteer leader broom is characterized as an infected branch that produces branches that grow erect and upright. Weeping brooms exhibit the opposite trait where branchlets droop and hang down below the infected branch at the point of infection. Tinnin and Knutson (1985) present a classification for *Pseudotsuga menziesii–Arceuthobium douglasii* pathosystem broom types, with illustrations in Parks et al. (1999). These were described for a systemic dwarf mistletoe infection and appear to be much larger. The three types, I, II, and II are also determined by distance from bole. Type I's are found furthest from the bole causing severe droop and eventual breakage of the infected limb; this resembles our classic deformity. Type II is found much closer to the bole, where the supporting limb grows upright and supports a profusion of smaller, infected twigs. This is similar to the volunteer leader broom (Hawksworth, 1961). Type III's arise from infections very near to or directly from the tree bole, but the form is similar to Type II brooms.

Hawksworth and Wiens (1996) point out secondary infections, where a second infection occurs within an already infected branch or deformity, is rarely observed for the *Tsuga heterophylla–Arceuthobium tsugense* pathosystem. However, we frequently observed multiple infections within a single deformity, especially large classic brooms (Figure 1b). Often, branchlets distal to a deformity would grow towards the edges of the crown and a second infection, causing a small spindle, could be observed there.

The impacts of deformity abundance (as opposed to infection severity or incidence) and class on tree physiology and growth have not been explored in *Tsuga heterophylla*, but previous studies on infected *Pinus jeffreyi* Balf. and *P. ponderosa* in valuable recreation forests found deformity removal increased host vigour and extended life span (Lightle & Hawksworth, 1973; Scharpf et al., 1987). Stanton (2006) examined radial growth impacts from broom abundance in *P. ponderosa* and found that infection severity explained the majority of growth reductions in their model and that in oldest stand with the largest trees, deformity abundance appeared to have little to no impact. The impact of deformity abundance on *T. heterophylla* may be more significant than on dry-side *Pinus* spp. as tree growing conditions are more favourable (Waring & Franklin, 1979) and host vigour is associated with dwarf mistletoe vigour (Shaw et al., 2005).

Further modelling is needed to determine if these classes have implications for crown function, spread and intensification, physiological functioning, and if infection classes can be predicted based on location within the crown. These determinations could also help future attempts to assess infection impacts in the crowns of infected *Tsuga heterophylla*, either from the ground or within the tree. Small units of measurement, called 'foliar units', are often employed in crown mapping that allow a researcher to quantify leaves, bark, cambium, and wood on complex branches, based on previous destructive sampling, that is not time intensive (Van Pelt & Sillett, 2008). Despite the gaps in knowledge, deformity class may be able to serve a similar role. Classifying deformities was not time intensive and deformities

are known to influence host growth, survival, and vigour (Lightle & Hawksworth, 1973; Scharpf et al., 1987), although inclusion of this classification system into other surveys would require a preliminary destructive sampling effort.

4.4 | Sapwood

While the crown showed evidence for profound change to structure, we found almost no evidence of an effect or relationship between sapwood area, either at *f*-diameter or at base of the live crown, and our measures of infection severity (Figure 8). Meinzer et al. (2004) measured sapwood area in severely infected and uninfected *T. heterophylla* and found insignificant differences in sapwood area, suggesting alterations to leaf area over carbon allocation were more advantageous. It has been shown that sapwood area is tightly correlated to the live foliage area above it, especially when measured at the base of the live crown (Ishii et al., 2017; Shinozaki et al., 1964b; Waring et al., 1982). Lacking direct measures of leaf area or mass, we substituted the total number of live branches and found a stronger correlation to relative sapwood area at *f*-diameter and at base of the live crown and estimated an increase in relative area as total live branches increased (Figure 8).

4.5 | Shifts in crown form, implications for tree function

The changes in foliage, crown structure, deformity abundance and volume, and sapwood indicated that infected *Tsuga heterophylla* trees likely experience a reduction in capacity for growth due to increasing infection by *Arceuthobium tsugense*. Some studies have reported initial infections are associated with increases in bole diameter growth potentially due to deformity-caused increases in branch foliage, or that more vigorous trees are more likely to be infected and are growing more rapidly despite infection (Marias et al., 2014; Shaw et al., 2005). Ultimately, infections result in large reductions in height and bole diameter growth as infection severity increases (Bell et al., 2020; Marias et al., 2014; Muir & Hennon, 2007). Top-kill has also been attributed to severe *A. tsugense* infection (Muir & Hennon, 2007). As an obligate parasite, *A. tsugense* infection may be driving diversions of photoassimilate from growth-related processes to maintenance of infected branches and its own maintenance and reproductive needs (Logan et al., 2013). This further suggested some branches may be net water and nutrient sinks rather than sources. The reduction of photoassimilate available to infected trees for biomass accumulation may be a mechanism to explain previously reported reductions to bole diameter growth (Bell et al., 2020; Marias et al., 2014). Intensification is also shrinking the crown volume further suggesting growth inhibition.

Compensation for alterations in water conductance at the leaf level, have been observed in pruned *Pinus taeda* L. such that leaf-specific water conductance is maintained (Pataki et al., 1998). Meinzer et al. (2004) reported reductions to overall tree water use for severely infected *Tsuga heterophylla*, which appeared to be compensated for by reductions to branch foliage and live branches, resulting in maintenance of leaf-specific conductivity. Our findings supported the reduction of branch foliage, but not the reduction of live branches, which suggested reducing foliage was the preferred mechanism for compensation. Additionally, stem sapwood area remained unaffected by infection severity suggesting conductive tissues may not be altered to maintain water conductance. Remaining branch foliage was increasingly found distal to an infection likely compounding reduced photosynthetic capability and reduced water use efficiency (Marias et al., 2014; Meinzer et al., 2004). Simultaneously, infection intensification resulted in branches of infected trees supporting 1–70 individual infections. When this process was scaled to the whole tree however, we observed that these shifts in form and function were due to an exceptionally small amount of deformed tissue. For example, in tree 7, where we observed the highest incidence by far, total deformity volume only reached a maximum of ~76 m^3, representing a mere 9% of total crown volume and yet almost all the live foliage was found distal to an infection (Figure 10). Most of the crown volume of trees was likely comprised of woody tissues or space, and minimally, actively photosynthesizing tissues. Therefore, the modest increase in the proportion of crown volume comprised of deformities seemed minor compared to the total volume, but likely represented almost all of the physiologically relevant tissues in the most severely infected trees.

The outsized impact of *Arceuthobium tsugense*, relative to the size of its host is phenomenal, especially when compared with the large leafy mistletoes in Loranthaceae. *Arceuthobium tsugense* plants grow to 7 cm in height on average and the plant itself is completely inconspicuous without careful observation of deformities high in the crowns of *Tsuga tsugense* or one of its occasional hosts (Hawksworth & Wiens, 1996). The leaves of the plant are quite reduced and are thought to perform only minor photosynthesis (Hawksworth & Wiens, 1996). However, one infection can produce large deformations in branch form and severely impact growth (Marias et al., 2014; Meinzer et al., 2004). In contrast, species of mistletoe in the *Amyema* genus, are much larger, producing robust, shrub-like plants that are on average 0.5–1 m in overall diameter (Shaw et al., 2004). Additionally, the mistletoe leaves in Australia are an important food and water source for birds and mammals (Shaw et al., 2004; Watson, 2001). *Amyema* spp. produce characteristic impacts to tree form, namely shrubby clumps at the site of infection and branch mortality distal to the infection point (Shaw et al., 2004). Tennakoon and Pate (1996) described the impacts of *Amyema preisii* (Miq.) Tiegh. infection on *Acacia acuminata* Benth. branches and found similar impacts to host branches as those in this study. As infection progressed, *Amyema preissii* foliage increased in parallel with declining host branch foliage distal to infection, ultimately resulting in death of the distal portion of the branch. The degree of these impacts to their host's tree form or growth however, is minimal compared to *A. tsugense* infections (Shaw et al., 2004).

4.5.1 | Incidence and severity model performance

This study was the first to provide a complete survey of all infections within a tree crown of an infected old-growth *Tsuga heterophylla*. However, the incidence of *Arceuthobium tsugense* infection did not adequately explain the impacts to crown architecture in our study when used alone in a model with a sample across a range of infection severity. Incidence may need to be qualified with a measure of severity, as a high concentration of infections on one branch would not have the same magnitude of physiological influence on water use dynamics as the same number of infections spread among many live branches (Meinzer et al., 2004). Comparisons of two *T. heterophylla* with the same or similar severity ratings could benefit from inclusion of incidence in models when considering impacts of intensification, such as our trees 7 and 12, both with branch severity measured at 100%. We observed an incidence of 3,615 infections in tree 7 and 813 in 12; this enormous difference in incidence likely results in very different influences on tree crown architecture. Stand- and tree-level characteristics common in forest modelling such as density, tree age and size, or tree vigour may also improve incidence model results (Geils et al., 2002; Muir et al., 2004). Attempts to model the epidemiology of *A. tsugense* could benefit from knowledge of incidence within the crown (Robinson & Geils, 2006), where location of female plants was crucial for determining spread within a tree or forest stand. Incidence is likely to be valuable for these applications of infection severity evaluation, but further investigation is required.

Discrepancies in model estimates and R^2 values, when using branch or foliage severity, suggested the effects of *Arceuthobium tsugense* may be better evaluated using one or the other of these severity measurements. In some cases, foliage severity may be more accurate estimating impacts such as average branch foliage or crown volume. In others, either measure may be inconsequential such as sapwood area, average branch deformity volume, or branch diameters and lengths. These differences likely highlight how infection impacts to crown form are manifested by the tree. For example, we found increasing infection severity to be associated with a decrease in branch foliage, and that the model with foliage severity as the explanatory variable had the highest R^2. So increasingly affected *Tsuga heterophylla* foliage by *A. tsugense* is likely to drive the reduction in average branch foliage cover, and not simply an increase in the number of infected branches. Future research that incorporates a larger sample size and includes the branch age and estimate of infection date, branch severity, foliage severity, and environmental explanatory variables in a model may further elucidate the degree to which infection severity transforms the crown of an infected *T. heterophylla*, thereby its physiology and further impacts to Northwest forests.

5 | CONCLUSIONS

The focus on a comprehensive description of *Tsuga heterophylla* crown architecture through a fine-scale gradient of infection severity by *Arceuthobium tsugense* utilizing tree climbing is novel in this field and has allowed new insight into the dwarf mistletoe–western hemlock pathosystems. Results from this study suggested that as the number of parasitic plants in infected *T. heterophylla* crowns increased, trees likely experienced a reduction in capacity for growth that coincided with an overall reduction in foliage amount, a shift of foliage distal to infection, and likely an increased resource demand by *A. tsugense* plants.

Previous research has often used the Hawksworth 6-class dwarf mistletoe rating (Hawksworth, 1977), dividing crowns into infection severity classes. This system is useful for forest managers seeking to sample large forest stands, where a fine-scale, infection severity measure is not a practical tool. However, it may overlook subtle transformations of the crown due to the subjective nature of evaluation (Shaw et al., 2000). The crown mapping technique can provide the fine-scale, infection severity measure in a research setting that eliminates some of this subjectivity. This technique can be prohibitively difficult in large, old trees requiring accessing the crown or felling trees which can compromise data due to crown damage. Despite these challenges, further implementation of the crown mapping technique as employed in this study has the potential to add significant clarity to the large, existing body of literature on the impacts of *A. tsugense* on *T. heterophylla* (Muir & Hennon, 2007).

ACKNOWLEDGEMENTS

We thank Russell Kramer, Mik Miazio, Elena Lauterbach, Kasey Swenson, Richard Tarkington, Madison Stone, Preston Durham, Jessica Jemison, Amanda Brackett, Matthew Aghai, Ryan Keeling, Brian French, Jimmy Swingle, Stan Pennors, Adam Sibley, Hannah Prather, Claire Brase, Katie Nicolato, Gabi Ritokova and Mark Schulze for invaluable help in the field. Henry Lee and McKenzie Vogel generously cross-dated our tree cores. Ariel Muldoon provided key experimental design, analysis and interpretation guidance. We also thank our two anonymous reviewers for their time and input. Data and facilities were provided by the HJ Andrews Experimental Forest and Long Term Ecological Research program, administered cooperatively by the USDA Forest Service Pacific Northwest Research Station, Oregon State University, and the Willamette National Forest. This material is based upon work supported by the National Science Foundation under Grant No. DEB-1440409. The Oregon State University Forest Health Lab provided funding for lodging and transportation. Funding for this work was also provided by the Oregon State University, College of Forestry Graduate Student Fellowship.

PEER REVIEW

The peer review history for this article is available at https://publons.com/publon/10.1111/efp.12664.

DATA AVAILABILITY STATEMENT

The data that support the findings of this study will soon be openly available in the HJ Andrews Data Catalog (URL: https://andrewsforest.oregonstate.edu/data).

ORCID

Stephen J. Calkins https://orcid.org/0000-0002-9160-0129
David C. Shaw https://orcid.org/0000-0002-3898-782X

REFERENCES

Agne, M. C., Shaw, D. C., Woolley, T. J., & Queijeiro-Bolãos, M. E. (2014). Effects of dwarf mistletoe on stand structure of lodgepole pine forests 21–28 years post-mountain pine beetle epidemic in central oregon. *PLoS One*, *9*(9), 21–28. https://doi.org/10.1371/journal.pone.0107532

Barton, K. (2019). *MuMIn: Multi-Model Inference*. R package version 1.43.15. Retrieved from https://CRAN.R-project.org/package=MuMIn

Bell, D. M., Pabst, R. J., & Shaw, D. C. (2020). Tree growth declines and mortality were associated with a parasitic plant during warm and dry climatic conditions in a temperate coniferous forest ecosystem. *Global Change Biology*, *26*(3), 1714–1724. https://doi.org/10.1111/gcb.14834

Dunham, P. A. (2008). *Incidence of insects, diseases, and other damaging agents in Oregon Forests*. Resour. Bull. PNW-RB-257 (89 pp). US Department of Agriculture, Forest Service, Pacific Northwest Research Station.

Fahey, R. T., Alveshere, B. C., Burton, J. I., D'Amato, A. W., Dickinson, Y. L., Keeton, W. S., Kern, C. C., Larson, A. J., Palik, B. J., Puettmann, K. J., Saunders, M. R., Webster, C. R., Atkins, J. W., Gough, C. M., & Hardiman, B. S. (2018). Shifting conceptions of complexity in forest management and silviculture. *Forest Ecology and Management*, *421*, 59–71. https://doi.org/10.1016/j.foreco.2018.01.011

Franklin, J. F., & Dyrness, C. T. (1973). *Natural Vegetation of Oregon and Washington*. Gen. Tech. Rep. PNW-GTR-008 (427 pp). U.S. Department of Agriculture, Forest Service, Pacific Northwest Research Station.

Franklin, J. F., Spies, T. A., Pelt, R. V., Carey, A. B., Thornburgh, D. A., Berg, D. R., Lindenmayer, D. B., Harmon, M. E., Keeton, W. S., Shaw, D. C., Bible, K., & Chen, J. (2002). Disturbances and structural development of natural forest ecosystems with silvicultural implications, using Douglas-fir forests as an example. *Forest Ecology and Management*, *155*(1–3), 399–423. https://doi.org/10.1016/S0378-1127(01)00575-8

Geils, B. W., Tovar, J. C., & Moody, B. (2002). *Mistletoes of North American conifers*. Gen. Tech. Rep. RMRS–GTR–98 (123 pp). U.S. Department of Agriculture, Forest Service, Rocky Mountain Research Station. https://doi.org/10.2737/RMRS-GTR-98

Glatzel, G., & Geils, B. W. (2009). Mistletoe Ecophysiology: Host-parasite Interactions. *Botany-Botanique*, *87*(1), 10–15. https://doi.org/10.1139/B08-096

Godfree, R. C., Tinnin, R. O., & Forbes, R. B. (2002). The effects of dwarf mistletoe, witches' brooms, stand structure, and site characteristics on the crown architecture of lodgepole pine in Oregon. *Canadian Journal of Forest Research*, *32*(8), 1360–1371. https://doi.org/10.1139/x02-058

Godfree, R. C., Tinnin, R. O., & Forbes, R. B. (2003). Relationships between dwarf mistletoe and the canopy structure of an old-growth lodgepole pine forest in central Oregon. *Canadian Journal of Forest Research*, *33*(6), 997–1009. https://doi.org/10.1139/x03-024

Griebel, A., Watson, D., & Pendall, E. (2017). Mistletoe, friend and foe: Synthesizing ecosystem implications of mistletoe infection. *Environmental Research Letters*, *12*(11), 115012. https://doi.org/10.1088/1748-9326/aa8fff

Hawksworth, F. G. (1961). Dwarf Mistletoe of Ponderosa Pine in the Southwest (p. 1246). *USDA Forest Service, Rocky Mountain Forest and Range Experiment Station, Technical Bulletin No. 1246*.

Hawksworth, F. G. (1977). *The 6-class dwarf mistletoe rating system*. USDA Forest Service General Technical Report, Rocky Mountain Forest and Range Experiment Station, RM-48.

Hawksworth, F. G., & Wiens, D. (1996). Dwarf mistletoes: Biology, pathology, and systematics. *Agriculture Handbook* (Vol. 709). https://doi.org/ISBN-13:978-92-95044-73-9s

Hoffman, C., Mathiasen, R., & Sieg, C. H. (2007). Dwarf mistletoe effects on fuel loadings in ponderosa pine forests in northern Arizona. *Canadian Journal of Forest Research*, *37*(3), 662–670. https://doi.org/10.1139/X06-259

Ishii, H. R., Sillett, S. C., & Carroll, A. L. (2017). Crown dynamics and wood production of Douglas-fir trees in an old-growth forest. *Forest Ecology and Management*, *384*, 157–168. https://doi.org/10.1016/j.foreco.2016.10.047

Ishii, H. R., Van Pelt, R., Parker, G. G., & Nadkarni, N. M. (2004). Age-related development of canopy structure and its ecological functions. In M. D. Lowman, & H. B. Rinker (Eds.), *Forest canopies* (2nd ed., pp. 102–117). Elsevier Academic Press. https://doi.org/10.1016/B978-012457553-0/50007-1

Kramer, R. D., Sillett, S. C., & Van Pelt, R. (2018). Quantifying aboveground components of *Picea sitchensis* for allometric comparisons among tall conifers in North American rainforests. *Forest Ecology and Management*, *430*(June), 59–77. https://doi.org/10.1016/j.foreco.2018.07.039

Lightle, P. C., & Hawksworth, F. G. (1973). *Control of dwarf mistletoe in a heavily used ponderosa pine recreation forest: Grand Canyon, Arizona*. USDA Forest Service. Research Paper, Rocky Mountain Forest Range Experimental Station, RM-106. Retrieved from https://www.biodiversitylibrary.org/item/178153

Logan, B. A., Reblin, J. S., Zonana, D. M., Dunlavey, R. F., Hricko, C. R., Hall, A. W., & Tissue, D. T. (2013). Impact of eastern dwarf mistletoe (*Arceuthobium pusillum*) on host white spruce (*Picea glauca*) development, growth and performance across multiple scales. *Physiologia Plantarum*, *147*(4), 502–513. https://doi.org/10.1111/j.1399-3054.2012.01681.x

Lutz, J. A., Furniss, T. J., Johnson, D. J., Davies, S. J., Allen, D., Alonso, A., Anderson-Teixeira, K. J., Andrade, A., Baltzer, J., Becker, K. M. L., Blomdahl, E. M., Bourg, N. A., Bunyavejchewin, S., Burslem, D. F. R. P., Cansler, C. A., Cao, K. E., Cao, M., Cárdenas, D., Chang, L.-W., … Zimmerman, J. K. (2018). Global importance of large-diameter trees. *Global Ecology and Biogeography*, *27*(7), 849–864. https://doi.org/10.1111/geb.12747

Marias, D. E., Meinzer, F. C., Woodruff, D. R., Shaw, D. C., Voelker, S. L., Brooks, J. R., Lachenbruch, B., Falk, K., & McKay, J. (2014). Impacts of dwarf mistletoe on the physiology of host *Tsuga heterophylla* trees as recorded in tree-ring C and O stable isotopes. *Tree Physiology*, *34*(6), 595–607. https://doi.org/10.1093/treephys/tpu046

Mathiasen, R. L., Nickrent, D. L., Shaw, D. C., & Watson, D. M. (2008). Mistletoes: Pathology, systematics, ecology, and management. *Plant Disease*, *92*(7), 988–1006. https://doi.org/10.1094/PDIS-92-7-0988

Meinzer, F. C., Woodruff, D. R., & Shaw, D. C. (2004). Integrated responses of hydraulic architecture, water and carbon relations of western hemlock to dwarf mistletoe infection. *Plant, Cell and Environment*, *27*(7), 937–946. https://doi.org/10.1111/j.1365-3040.2004.01199.x

Michel, A. K., & Winter, S. (2009). Tree microhabitat structures as indicators of biodiversity in Douglas-fir forests of different stand ages and management histories in the Pacific Northwest, U.S.A. *Forest Ecology and Management*, *257*(6), 1453–1464. https://doi.org/10.1016/j.foreco.2008.11.027

Muir, J. A., & Hennon, P. E. (2007). A synthesis of the literature on the biology, ecology, and management of Western Hemlock dwarf mistletoe. *USDA Forest Service - General Technical Report PNW-GTR*, *718*, 1–142. https://doi.org/10.2737/PNW-GTR-718

Muir, J. A., Robinson, D. C. E., & Geils, B. W. (2004). Characterizing the effects of dwarf mistletoe and other diseases for sustainable forest management. *BC Journal of Ecosystems and Management*, *3*(2).

Nakagawa, S., Johnson, P. C. D., & Schielzeth, H. (2017). The coefficient of determination R2 and intra-class correlation coefficient from generalized linear mixed-effects models revisited and expanded. *Journal of the Royal Society Interface*, *14*(134). https://doi.org/10.1098/rsif.2017.0213

Nakagawa, S., & Schielzeth, H. (2013). A general and simple method for obtaining R2 from generalized linear mixed-effects models. *Methods in Ecology and Evolution*, *4*(2), 133–142. https://doi.org/10.1111/j.2041-210x.2012.00261.x

Parks, C. G., Bull, E. L., Tinnin, R. O., Shepherd, J. F., & Blumton, A. K. (1999). Wildlife use of dwarf mistletoe brooms in Douglas-fir in Northeast Oregon. *Western Journal of Applied Forestry*, *14*, 100–105. https://doi.org/10.1093/wjaf/14.2.100

Parmeter, J. R. J. (1978). Forest stand dynamics and ecological factors in relation to dwarf mistletoe spread, impact, and control. In R. F. Scharpf, & J. R. J. Parmeter (Eds.), *Symposium on dwarf mistletoe control through forest management* (pp. 16–30). Berkeley.

Pataki, D. E., Oren, R., & Phillips, N. (1998). Responses of sap flux and stomatal conductance of *Pinus taeda* L. trees to stepwise reductions in leaf area. *Journal of Experimental Botany*, *49*(322), 871–878. https://doi.org/10.1093/jxb/49.322.871

R Core Team (2019). *R: A language and environment for statistical computing*. R Foundation for Statistical Computing. Retrieved from https://www.r-project.org/

Ramsey, F., & Schafer, D. (2012). *The statistical sleuth: A course in methods of data analysis*. Cengage Learning.

Reilly, M. J., & Spies, T. A. (2015). Regional variation in stand structure and development in forests of Oregon, Washington, and inland Northern California. *Ecosphere*, *6*(10), 1–27. https://doi.org/10.1890/ES14-00469.1

Reilly, M. J., & Spies, T. A. (2016). Disturbance, tree mortality, and implications for contemporary regional forest change in the Pacific Northwest. *Forest Ecology and Management*, *374*, 102–110. https://doi.org/10.1016/j.foreco.2016.05.002

Robinson, D. C. E., & Geils, B. W. (2006). Modeling dwarf mistletoe at three scales: Life history, ballistics and contagion. *Ecological Modeling*, *199*(1), 23–28. https://doi.org/10.1016/j.ecolmodel.2006.06.007

Sala, A., Carey, E. V., & Callaway, R. M. (2001). Dwarf mistletoe affects whole-tree water relations of Douglas fir and western larch primarily through changes in leaf to sapwood ratios. *Oecologia*, *126*(1), 42–52. https://doi.org/10.1007/s004420000503

Scharpf, R. F., Smith, R. S., & Vogler, D. (1987). *Pruning dwarf mistletoe brooms reduces stress on Jeffrey pines, Cleveland National Forest, California*. USDA Forest Service Research Paper, Pacific Southwest Forest and Range Experiment Station, PSW-186.

Shaw, D. C., & Agne, M. C. (2017). Fire and dwarf mistletoe (Viscaceae: *Arceuthobium* species) in western north America: Contrasting *Arceuthobium tsugense* and *Arceuthobium americanum*. *Botany-Botanique*, *95*(3), 231–246. https://doi.org/10.1139/cjb-2016-0245

Shaw, D. C., Chen, J., Freeman, E. A., & Braun, D. M. (2005). Spatial and population characteristics of dwarf mistletoe infected trees in an old-growth Douglas-fir - western hemlock forest. *Canadian Journal of Forest Research*, *35*(4), 990–1001. https://doi.org/10.1139/x05-022

Shaw, D. C., Edmonds, R. L., Littke, W. R., Browning, J. E., & Russel, K. W. (1995). Incidence of wetwood and decay in precommercially thinned western hemlock stands. *Canadian Journal of Forest Research*, *25*, 1269–1277. https://doi.org/10.1139/x95-140

Shaw, D. C., Freeman, E. A., & Mathiasen, R. L. (2000). Evaluating the accuracy of ground-based hemlock dwarf mistletoe rating: A case study using the wind river canopy crane. *Western Journal of Applied Forestry*, *15*, 8–14. https://doi.org/10.1093/wjaf/15.1.8

Shaw, D. C., Huso, M., & Bruner, H. (2008). Basal area growth impacts of dwarf mistletoe on western hemlock in an old-growth forest. *Canadian Journal of Forest Research*, *38*(3), 576–583. https://doi.org/10.1139/X07-174

Shaw, D. C., & Mathiasen, R. L. (2013). Forest diseases caused by higher parasitic plants: Mistletoes. In *Infectious forest diseases* (pp. 97–114). CABI Publishing. https://doi.org/10.1079/9781780640402.0097

Shaw, D. C., Watson, D. M., & Mathiasen, R. L. (2004). Comparison of dwarf mistletoes (*Arceuthobium* spp., Viscaceae) in the western United States with mistletoes (*Amyema* spp., Loranthaceae) in Australia - Ecological analogs and reciprocal models for ecosystem management. *Australian Journal of Botany*, *52*(4), 481–498. https://doi.org/10.1071/BT03074

Shaw, D. C., & Weiss, S. B. (2000). Canopy Light and the Distribution of Hemlock Dwarf Mistletoe (*Arceuthobium tsugense* [Rosendahl] G.N. Jones subsp. *tsugense*) Aerial Shoots in an Old-rowth Douglas-fir/Western Hemlock Forest. *Northwest Science*, *74*(4), 306–315.

Shinozaki, K., Yoda, K., Hozumi, K., & Kira, T. (1964a). A quantitative analysis of plant form-the pipe model theory: I. Basic analyses. *Japanese Journal of Ecology*, *14*(3), 97–105. https://doi.org/10.18960/seitai.14.3_97

Shinozaki, K., Yoda, K., Hozumi, K., & Kira, T. (1964b). A quantitative analysis of plant form-the pipe model theory: II. Further evidence of the theory and its application in forest ecology. *Japanese Journal of Ecology*, *14*(4), 133–139. https://doi.org/10.18960/seitai.14.4_133

Sillett, S. C., Van Pelt, R., Koch, G. W., Ambrose, A. R., Carroll, A. L., Antoine, M. E., & Mifsud, B. M. (2010). Increasing wood production through old age in tall trees. *Forest Ecology and Management*, *259*(5), 976–994. https://doi.org/10.1016/j.foreco.2009.12

Smith, R. (1969). Assessing dwarf mistletoe on western hemlock. *Forest Science*, *15*(3), 277–285. https://doi.org/10.1093/forestscience/15.3.277

Smith, W. K., & Brewer, C. A. (1994). The adaptive importance of shoot and crown architecture in conifer trees. *The American Naturalist*, *143*(3), 528–532. https://doi.org/10.1086/285618

Spies, T. A. (2016). *LiDAR data (October 2011) for the Upper Blue River Watershed, Willamette National Forest*. Long-Term Ecological Research. Forest Science Data Bank. [Database]. Retrieved from http://andlter.forestry.oregonstate.edu/data/abstract.aspx?dbcode=GI011. https://doi.org/10.6073/pasta/8e4f57bafaaad5677977dee51bb3077c. Accessed 2020-07-28

Spies, T. A., & Franklin, J. F. (1991). *The Structure of Natural Young, Mature, and Old-Growth Douglas-fir Forests in Oregon and Washington*. USDA Forest Service General Technical Report PNW-GTR-285. https://doi.org/10.1111/1750-3841.12978

Spies, T. A., Stine, P. A., Gravenmier, R., Long, J. W., & Reilly, M. J. (2018). *Synthesis of Science to Inform Land Management Within the Northwest Forest Plan Area. Gen. Tech. Rep. PNW-GTR_966*, *1*(June), 1020.

Stanton, S. (2006). The differential effects of dwarf mistletoe infection and broom abundance on the radial growth of managed ponderosa pine. *Forest Ecology and Management*, *223*, 318–326. https://doi.org/10.1016/j.foreco.2005.11.011

Swanson, F. J., & Jones, J. A. (2002). Geomorphology and hydrology of the HJ Andrews experimental forest, Blue River, Oregon. *Field Guide to Geologic Processes in Cascadia, Oregon Department of Geology and Minderal Industries, Special Paper*, *36*, 289–313.

Swanson, M. E., Shaw, D. C., & Marosi, T. K. (2006). Distribution of western hemlock dwarf mistletoe (*Arceuthobium tsugense* [Rosendahl] G.N. Jones subsp. *tsugense*) in mature and old-growth douglas-fir (*Pseudotsuga menziesii* [Mirb.] Franco) forests. *Northwest Science*, *80*(3), 207–217.

Tennakoon, K. U., & Pate, J. S. (1996). Effects of parasitism by a mistletoe on the structure and functioning of branches of its host. *Plant, Cell and Environment*, *19*, 517–528. https://doi.org/10.1111/j.1365-3040.1996.tb00385.x

Tepley, A. J., Swanson, F. J., & Spies, T. A. (2013). Fire-mediated pathways of stand development in Douglas-fir/western hemlock forests of the Pacific Northwest, USA. *Ecology*, *94*(8), 1729–1743. https://doi.org/10.1890/12-1506.1

Tinnin, R. O., & Knutson, D. M. (1985). *How to identify brooms in Douglas-fir caused by dwarf mistletoe*. Research Note PNW-426, USDA Forest Service, Pacific Northwest Research Station, Portland, OR.

Van Pelt, R., & Nadkarni, N. M. (2004). Development of canopy structure in *Pseudotsuga menziesii* forests in the southern Washington Cascades. *Forest Science*, *50*(3), 326–341. https://doi.org/10.1093/forestscience/50.3.326

Van Pelt, R., & North, M. P. (1999). Testing a ground-based canopy model using the Wind River Canopy Crane. *Selbyana*, *20*(2), 357–362.

Van Pelt, R., & Sillett, S. C. (2008). Crown development of coastal *Pseudotsuga menziesii*, including a conceptual model for tall conifers. *Ecological Monographs*, *78*(2), 283–311. https://doi.org/10.1890/07-0158.1

Van Pelt, R., Sillett, S. C., & Nadkarni, N. M. (2004). Quantifying and visualizing canopy structure in tall forests. Methods and a case study. In M. D. Lowman, & H. B. Rinker (Eds.), *Forest canopies* (2nd ed., pp. 49–72). Elsevier Academic Press. https://doi.org/10.1016/B978-012457553-0/50007-1

Venables, W. N., & Ripley, B. D. (2002). *Modern applied statistics with S* (4th ed.). Springer. ISBN 0-387-95457-0.

Waring, R. H., & Franklin, J. F. (1979). Evergreen coniferous forests of the Pacific Northwest. *American Association for the Advancement of Science*, *204*(4400), 1380–1386. https://doi.org/10.1126/science.204.4400.1380

Waring, R. H., Schroeder, P. E., & Oren, R. (1982). Application of the pipe model theory to predict canopy leaf area. *Canadian Journal of Forest Research*, *12*(3), 556–560. https://doi.org/10.1139/x82-086

Watson, D. M. (2001). Mistletoe - A keystone resource in forests and woodlands worldwide. *Annual Review of Ecology and Systematics*, *32*(1), 219–249. https://doi.org/10.1146/annurev.ecolsys.32.081501.114024

Wellwood, R. W. (1956). Some effects of dwarf mistletoe on western hemlock. *The Forestry Chronicle*, *32*(3), 282–296. https://doi.org/10.5558/tfc32282-3

Zald, H. S. J., Spies, T. A., Seidl, R., Pabst, R. J., Olsen, K. A., & Steel, E. A. (2016). Complex mountain terrain and disturbance history drive variation in forest aboveground live carbon density in the western Oregon Cascades, USA. *Forest Ecology and Management*, *366*, 193–207. https://doi.org/10.1016/j.foreco.2016.01.036

How to cite this article: Calkins SJ, Shaw DC, Lan Y-H. Transformation of western hemlock (*Tsuga heterophylla*) tree crowns by dwarf mistletoe (*Arceuthobium tsugense*, Viscaceae). *Forest Pathology*. 2020;00:e12664. https://doi.org/10.1111/efp.12664

APPENDIX A

FULL SET OF MODEL RESULTS FOR THE BRANCH-RELATED RESPONSE VARIABLES

The estimated slope, 95% confidence intervals, test statistics and R^2 for each fixed effect and response variable. Coefficient estimates represent a shift from 0% to 100% for branch and foliage severity and a shift from 0 to 100 infections for incidence.

Response	Model Type	Fixed Effect	Coefficient Estimate	Low 95% CI	High 95% CI	*F*	*df*	χ^2	*p*	R^2
Average Branch Diameter	LM	Branch Severity	0.05	−1.08	1.17	0.01	1, 14	---	0.931	0.00
		Foliage Severity	−0.02	−1.13	1.09	0.00	1, 14	---	0.969	0.00
		Incidence	0.00	0.00	0.00	0.10	1, 14	---	0.757	0.01
Median Branch Diameter	LM	Branch Severity	0.02	−1.03	1.07	0.00	1, 14	---	0.967	0.00
		Foliage Severity	0.02	−1.01	1.05	0.00	1, 14	---	0.971	0.00
		Incidence	0.01	−0.03	0.05	0.29	1, 14	---	0.599	0.02
Max Branch Diameter	LM	Branch Severity	0.60	−2.64	3.84	0.16	1, 14	---	0.697	0.01
		Foliage Severity	0.29	−2.90	3.49	0.04	1, 14	---	0.847	0.00
		Incidence	0.00	−0.14	0.14	0.00	1, 14	---	0.960	0.00
Average Branch Length	LM	Branch Severity	−0.33	−1.08	0.43	0.86	1, 14	---	0.370	0.06
		Foliage Severity	−0.30	−1.05	0.44	0.76	1, 14	---	0.397	0.05
		Incidence	0.01	0.00	0.00	0.65	1, 14	---	0.432	0.04
Median Branch Length	LM	Branch Severity	−0.39	−1.14	0.36	1.26	1, 14	---	0.280	0.08
		Foliage Severity	−0.36	−1.10	0.38	1.25	1, 14	---	0.311	0.07
		Incidence	0.00	−0.02	0.04	0.32	1, 14	---	0.582	0.02
Max Branch Length	LM	Branch Severity	−0.99	−2.81	0.83	1.35	1, 14	---	0.264	0.09
		Foliage Severity	−0.94	−2.73	0.86	1.25	1, 14	---	0.282	0.08
		Incidence	0.02	−0.06	0.10	0.19	1, 14	---	0.673	0.01
Average Slope 1	LM	Branch Severity	7.02	−0.56	14.61	3.95	1, 14	---	0.067	0.22
		Foliage Severity	4.53	−3.50	12.55	1.46	1, 14	---	0.246	0.09
		Incidence	0.17	−0.19	0.52	1.01	1, 14	---	0.331	0.07
Median Slope 1	LM	Branch Severity	7.04	−0.40	14.48	4.11	1, 14	---	0.062	0.23
		Foliage Severity	5.02	−2.78	12.82	1.90	1, 14	---	0.189	0.12
		Incidence	0.17	−0.18	0.52	1.09	1, 14	---	0.315	0.07
Average Slope 2	LM	Branch Severity	−6.88	−22.77	9.01	0.86	1, 14	---	0.369	0.06
		Foliage Severity	−11.73	−26.33	2.88	2.97	1, 14	---	0.107	0.17
		Incidence	−0.17	−0.86	0.52	0.28	1, 14	---	0.605	0.02
Median Slope 2	LM	Branch Severity	−8.03	−24.88	8.82	1.04	1, 14	---	0.324	0.07
		Foliage Severity	−13.51	−28.81	1.80	3.58	1, 14	---	0.079	0.20
		Incidence	−0.20	−0.94	0.53	0.35	1, 14	---	0.562	0.02
Average Branch Foliage	LM	Branch Severity	−10.96	−18.55	−3.38	9.61	1, 14	---	0.008	0.41
		Foliage Severity	−13.39	−19.27	−7.51	23.82	1, 14	---	0.000	0.63
		Incidence	−0.32	−0.69	0.06	3.17	1, 14	---	0.097	0.18
Number of Live Branches	GLM	Branch Severity	0.76	0.55	1.06	---	1	2.35	0.126	0.14
		Foliage Severity	0.76	0.55	1.06	---	1	2.46	0.117	0.14
		Incidence	1.00	0.99	1.02	---	1	0.01	0.931	0.00
Number of Dead Branches	GLM	Branch Severity	1.36	0.89	2.08	---	1	1.88	0.170	0.11
		Foliage Severity	1.37	0.92	2.04	---	1	2.20	0.138	0.13
		Incidence	1.01	1.00	1.03	---	1	2.48	0.115	0.14
Total Number of Branches	GLM	Branch Severity	0.86	0.67	1.10	---	1	1.43	0.232	0.09
		Foliage Severity	0.87	0.68	1.10	---	1	1.31	0.253	0.08
		Incidence	1.00	0.99	1.01	---	1	0.43	0.512	0.03

Response	Model Type	Fixed Effect	Coefficient Estimate	Low 95% CI	High 95% CI	*F*	*df*	χ^2	*p*	R^2
Live Proportion	GLM	Branch Severity	0.56	0.29	1.05	3.26	1, 14	---	0.090	0.01
		Foliage Severity	0.55	0.30	1.01	3.74	1, 14	---	0.070	0.01
		Incidence	0.99	0.96	1.01	0.84	1, 14	---	0.380	0.00

APPENDIX B

FULL SET OF MODEL RESULTS FOR THE DEFORMITY-RELATED RESPONSE VARIABLES

The estimated slope, 95% confidence intervals, test statistics and R^2 for each fixed effect and response variable. Coefficient estimates represent a shift from 0% to 100% for branch and foliage severity and a shift from 0 to 100 infections for incidence.

Response	Model Type	Fixed Effect	Coefficient Estimate	Low 95% CI	High 95% CI	*F*	*df*	χ^2	*p*	R^2
Average Deformity Distance to Bole	LM	Branch Severity	3.17	1.62	4.70	19.43	1, 14	---	0.001	0.58
		Foliage Severity	2.29	0.36	4.22	6.47	1, 14	---	0.023	0.32
		Incidence	0.11	0.02	0.19	7.81	1, 14	---	0.014	0.36
Average Branch Deformity Volume	LM	Branch Severity	0.09	−0.20	0.37	0.49	1, 14	---	0.501	0.05
		Foliage Severity	0.09	−0.10	0.28	1.21	1, 14	---	0.299	0.12
		Incidence	0.00	0.00	0.00	0.06	1, 14	---	0.808	0.01
Total Deformity Volume	LM	Branch Severity	49.40	22.63	76.17	15.67	1, 14	---	0.001	0.53
		Foliage Severity	55.12	33.54	76.70	30	1, 14	---	0.000	0.68
		Incidence	---	---	---	---	1, 14	---	---	---
Proportion of Crown in Deformity	LM	Branch Severity	0.06	0.02	0.10	10.24	1, 14	---	0.006	0.42
		Foliage Severity	0.07	0.04	0.11	18.85	1, 14	---	0.001	0.57
		Incidence	---	---	---	---	1, 14	---	---	---
Median Dwarf Mistletoe Infection	GLM	Branch Severity	27.20	9.60	90.06	---	1	23.98	0.000	0.78
		Foliage Severity	14.12	5.67	37.85	---	1	17.88	0.000	0.67
		Incidence	1.11	1.05	1.20	---	1	10.89	0.001	0.49

APPENDIX C

FULL SET OF MODEL RESULTS FOR THE WHOLE TREE AND SAPWOOD-RELATED RESPONSE VARIABLES

The estimated slope, 95% confidence intervals, test statistics and R^2 for each fixed effect and response variable. Coefficient estimates represent a shift from 0% to 100% for branch and foliage severity and a shift from 0 to 100 infections for incidence.

Response	Model Type	Fixed Effect	Coefficient Estimate	Low 95% CI	High 95% CI	*F*	*df*	χ^2	*p*	R^2
Minimum Branch Height	LM	Branch Severity	2.49	−2.60	7.57	1.1	1, 14	---	0.312	0.07
		Foliage Severity	2.44	−2.55	7.44	1.1	1, 14	---	0.312	0.07
		Incidence	−0.02	−0.24	0.21	0.03	1, 14	---	0.873	0.00
Crown Depth	LM	Branch Severity	−6.25	−13.19	0.70	3.72	1, 14	---	0.074	0.21
		Foliage Severity	−5.77	−12.70	1.15	3.19	1, 14	---	0.096	0.19
		Incidence	−0.11	−0.44	0.21	0.55	1, 14	---	0.470	0.04
Frusta-based Crown Volume	LM	Branch Severity	−632.87	−1,330.30	64.57	5.46	1, 14	---	0.072	0.21
		Foliage Severity	−696.34	−1,357.10	−35.58	7.72	1, 14	---	0.040	0.27
		Incidence	−2.38	−35.40	31.14	0.12	1, 14	---	0.881	0.00
Sapwood Area at f DBH	LM	Branch Severity	−0.04	−0.09	0.02	1.74	1, 14	---	0.208	0.11
		Foliage Severity	−0.03	−0.09	0.03	1.33	1, 14	---	0.269	0.09
		Incidence	0.00	0.00	0.00	0.06	1, 14	---	0.804	0.00

Response	Model Type	Fixed Effect	Coefficient Estimate	Low 95% CI	High 95% CI	*F*	*df*	χ^2	*p*	R^2
Relative Sapwood Area at f-DBH	LM	Branch Severity	−0.02	−0.24	0.19	0.06	1, 14	---	0.816	0.00
		Foliage Severity	−0.04	−0.25	0.17	0.16	1, 14	---	0.694	0.01
		Incidence	0.00	0.00	0.00	0.02	1, 14	---	0.891	0.00
Sapwood Area at Live Crown Base	LM	Branch Severity	−0.03	−0.08	0.02	1.52	1, 14	---	0.239	0.10
		Foliage Severity	−0.02	−0.07	0.03	1.00	1, 14	---	0.334	0.07
		Incidence	0.00	0.00	0.00	0.02	1, 14	---	0.898	0.00
Relative Sapwood Area at Live Crown Base	LM	Branch Severity	−0.02	−0.19	0.15	0.04	1, 14	---	0.838	0.00
		Foliage Severity	−0.01	−0.18	0.16	0.02	1, 14	---	0.890	0.00
		Incidence	0.00	0.00	0.00	0.04	1, 14	---	0.844	0.00